Target Atmospheric CO_2: Where Should Humanity Aim?

James Hansen,[1,2*] Makiko Sato,[1,2] Pushker Kharecha,[1,2] David Beerling,[3]
Valerie Masson-Delmotte,[4] Mark Pagani,[5] Maureen Raymo,[6] Dana L. Royer,[7] James C. Zachos[8]

Paleoclimate data show that climate sensitivity is ~3°C for doubled CO_2, including only fast feedback processes. Equilibrium sensitivity, including slower surface albedo feedbacks, is ~6°C for doubled CO_2 for the range of climate states between glacial conditions and ice-free Antarctica. Decreasing CO_2 was the main cause of a cooling trend that began 50 million years ago, large scale glaciation occurring when CO_2 fell to 425±75 ppm, a level that will be exceeded within decades, barring prompt policy changes. If humanity wishes to preserve a planet similar to that on which civilization developed and to which life on Earth is adapted, paleoclimate evidence and ongoing climate change suggest that CO_2 will need to be reduced from its current 385 ppm to at most 350 ppm. The largest uncertainty in the target arises from possible changes of non-CO_2 forcings. An initial 350 ppm CO_2 target may be achievable by phasing out coal use except where CO_2 is captured and adopting agricultural and forestry practices that sequester carbon. If the present overshoot of this target CO_2 is not brief, there is a possibility of seeding irreversible catastrophic effects.

Human activities are altering Earth's atmospheric composition. Concern about global warming due to long-lived human-made greenhouse gases (GHGs) led to the United Nations Framework Convention on Climate Change (1) with the objective of stabilizing GHGs in the atmosphere at a level preventing "dangerous anthropogenic interference with the climate system."

The Intergovernmental Panel on Climate Change (IPCC, 2) and others (3) used several "reasons for concern" to estimate that global warming of more than 2-3°C may be dangerous. The European Union adopted 2°C above pre-industrial global temperature as a goal to limit human-made warming (4). Hansen et al. (5) argued for a limit of 1°C global warming (relative to 2000, 1.7°C relative to pre-industrial time), aiming to avoid practically irreversible ice sheet and species loss. This 1°C limit, with nominal climate sensitivity of ¾°C per W/m^2 and plausible control of other GHGs (6), implies maximum CO_2 ~ 450 ppm (5).

Our current analysis suggests that humanity must aim for an even lower level of GHGs. Paleoclimate data and ongoing global changes indicate that 'slow' climate feedback processes not included in most climate models, such as ice sheet disintegration, vegetation migration, and GHG release from soils, tundra or ocean sediments, may begin to come into play on time scales as short as centuries or less (7). Rapid on-going climate changes and realization that Earth is out of energy balance, implying that more warming is 'in the pipeline' (8), add urgency to investigation of the dangerous level of GHGs.

A probabilistic analysis (9) concluded that the long-term CO_2 limit is in the range 300-500 ppm for 25 percent risk tolerance, depending on climate sensitivity and non-CO_2 forcings.

---

[1]NASA/Goddard Institute for Space Studies, New York, NY 10025, USA. [2]Columbia University Earth Institute, New York, NY 10027, USA. [3]Dept. Animal and Plant Sciences, University of Sheffield, Sheffield S10 2TN, UK. [4]Lab. des Sciences du Climat et l'Environnement/Institut Pierre Simon Laplace, CEA-CNRS-Universite de Versailles Saint-Quentin en Yvelines, CE Saclay, 91191, Gif-sur-Yvette, France. [5]Dept. Geology and Geophysics, Yale University, New Haven, CT 06520-8109, USA. [6]Dept. Earth Sciences, Boston University, Boston, MA 02215, USA. [7]Dept. Earth and Environmental Sciences, Wesleyan University, Middletown, CT 06459-0139, USA. [8]Earth & Planetary Sciences Dept., University of California, Santa Cruz, Santa Cruz, CA 95064, USA.

*To whom correspondence should be addressed. E-mail: jhansen@giss.nasa.gov

Stabilizing atmospheric CO_2 and climate requires that net CO_2 emissions approach zero (10), because of the long lifetime of CO_2.

We use paleoclimate data to show that long-term climate has high sensitivity to climate forcings and that the present global mean CO_2, 385 ppm, is already in the dangerous zone. Despite rapid current CO_2 growth, ~2 ppm/year, we show that it is conceivable to lower CO_2 this century to less than the current amount, but only via prompt policy changes.

Climate sensitivity. A global climate forcing, measured in W/m^2 averaged over the planet, is an imposed perturbation of the planet's energy balance. Increase of solar irradiance (So) by 2% and doubling of atmospheric CO_2 are each forcings of about 4 W/m^2 (11).

Charney (12) defined an idealized climate sensitivity problem, asking how much global surface temperature would increase if atmospheric CO_2 were instantly doubled, assuming that slowly-changing planetary surface conditions, such as ice sheets and forest cover, were fixed. Long-lived GHGs, except for the specified CO_2 change, were also fixed, not responding to climate change. The Charney problem thus provides a measure of climate sensitivity including only the effect of 'fast' feedback processes, such as changes of water vapor, clouds and sea ice.

Classification of climate change mechanisms into fast and slow feedbacks is useful, even though time scales of these changes may overlap. We include as fast feedbacks aerosol changes, e.g., of desert dust and marine dimethylsulfide, that occur in response to climate change (7).

Charney (12) used climate models to estimate fast-feedback doubled CO_2 sensitivity of 3 ± 1.5°C. Water vapor increase and sea ice decrease in response to global warming were both found to be strong positive feedbacks, amplifying the surface temperature response. Climate models in the current IPCC (2) assessment still agree with Charney's estimate.

Climate models alone are unable to define climate sensitivity more precisely, because it is difficult to prove that models realistically incorporate all feedback processes. The Earth's history, however, allows empirical inference of both fast feedback climate sensitivity and long-term sensitivity to specified GHG change including the slow ice sheet feedback.

Pleistocene Epoch.

Atmospheric composition and surface properties in the late Pleistocene are known well enough for accurate assessment of the fast-feedback (Charney) climate sensitivity. We first compare the pre-industrial Holocene with the last glacial maximum [LGM, 20 ky BP (before present)]. The planet was in energy balance in both periods within a small fraction of 1 W/m^2, as shown by considering the contrary: an imbalance of 1 W/m^2 maintained a few millennia would melt all ice on the planet or change ocean temperature an amount far outside measured variations (Table S1 of 8). The approximate equilibrium characterizing most of Earth's history is unlike the current situation, in which GHGs are rising at a rate much faster than the coupled climate system can respond.

Climate forcing in the LGM equilibrium state due to the slow-feedback ice age surface properties, i.e., increased ice area, different vegetation distribution, and continental shelf exposure, was -3.5 ± 1 W/m^2 (13) relative to the Holocene. Additional forcing due to reduced amounts of long-lived GHGs (CO_2, CH_4, N_2O), including the indirect effects of CH_4 on tropospheric ozone and stratospheric water vapor (fig. S1) was -3 ± 0.5 W/m^2. Global forcing due to slight changes in the Earth's orbit is a negligible fraction of 1 W/m^2 (fig. S2). The total 6.5 W/m^2 forcing and global surface temperature change of 5 ± 1°C relative to the Holocene (14, 15) yield an empirical sensitivity ~¾ ± ¼ °C per W/m^2 forcing, i.e., a Charney sensitivity of 3 ± 1 °C for the 4 W/m^2 forcing of doubled CO_2. This empirical fast-feedback climate sensitivity allows water vapor, clouds, aerosols, sea ice, and all other fast feedbacks that exist in the real world to respond naturally to global climate change.

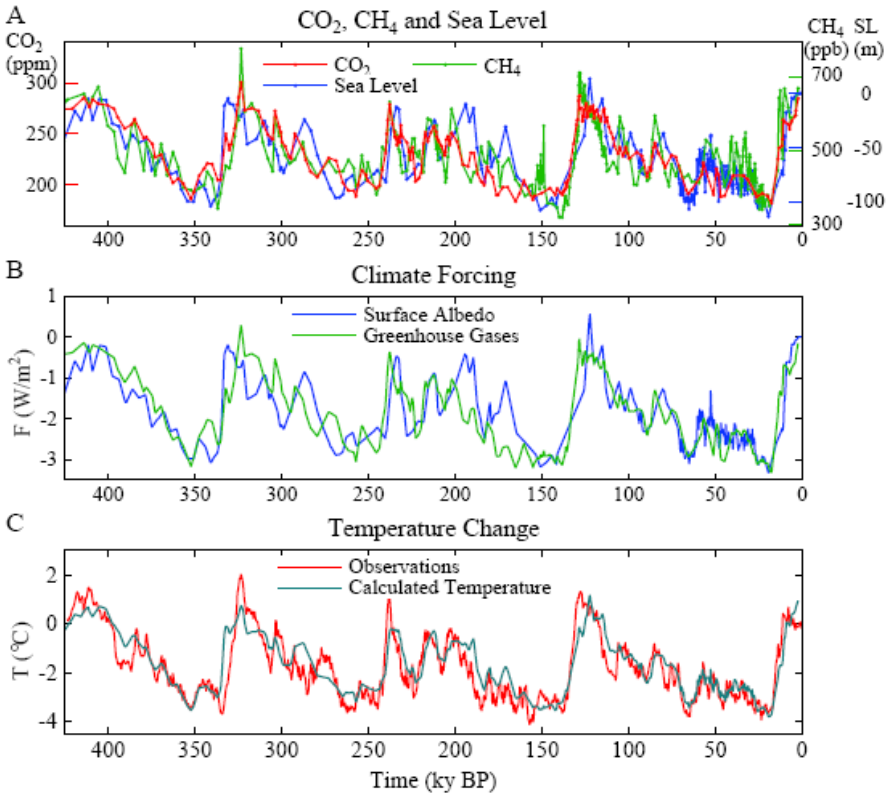

Fig. 1. (A) CO_2, CH_4 (16) and sea level (17) for past 425 ky. (B) Climate forcings due to changes of GHGs and ice sheet area, the latter inferred from sea level change. (C) Calculated global temperature change based on climate sensitivity of ¾°C per W/m^2. Observations are Antarctic temperature change (16) divided by two.

Climate sensitivity varies as Earth becomes warmer or cooler. Toward colder extremes, as the area of sea ice grows, the planet approaches runaway snowball-Earth conditions, and at high temperatures it can approach a runaway greenhouse effect (11). At its present temperature Earth is on a flat portion of its fast-feedback climate sensitivity curve (fig. S3). Thus our empirical sensitivity, although strictly the mean fast-feedback sensitivity for climate states ranging from the ice age to the current interglacial period, is also today's fast-feedback climate sensitivity.

Verification. Our empirical fast-feedback climate sensitivity, derived by comparing conditions at two points in time, can be checked over the longer period of ice core data. Fig. 1A shows CO_2 and CH_4 data from the Antarctic Vostok ice core (16) and sea level based on Red Sea sediment cores (17). Gases are from the same ice core and have a consistent time scale, but dating with respect to sea level may have errors up to several thousand years.

We use the GHG and sea level data to calculate climate forcing by GHGs and surface albedo change as in prior calculations (7), but with two refinements. First, we specify the N_2O climate forcing as 12 percent of the sum of the CO_2 and CH_4 forcings, rather than the 15 percent estimated earlier (7) Because N_2O data are not available for the entire record, and its forcing is small and highly correlated with CO_2 and CH_4, we take the GHG effective forcing as

$$Fe\ (GHGs) = 1.12\ [Fa(CO_2) + 1.4\ Fa(CH_4)], \qquad (1)$$

using published formulae for Fa of each gas (18). The factor 1.4 accounts for the higher efficacy of CH_4 relative to CO_2, which is due mainly to the indirect effect of CH_4 on tropospheric ozone and stratospheric water vapor (11). The resulting GHG forcing between the LGM and late Holocene is 3 W/m^2, apportioned as 75% CO_2, 14% CH_4 and 11% N_2O.

The second refinement in our calculations is to surface albedo. Based on models of ice sheet shape, we take the horizontal area of the ice sheet as proportional to the 4/5 power of volume. Fig. S4 compares our present albedo forcing with prior use (7) of exponent 2/3, showing that this choice and division of the ice into multiple ice sheets has only a minor effect.

Multiplying the sum of GHG and surface albedo forcings by climate sensitivity ¾°C per W/m^2 yields the blue curve in Fig. 1(C). Vostok temperature change (16) divided by two (red curve) is used to crudely estimate global temperature change, as typical glacial-interglacial global annual-mean temperature change is ~5°C and is associated with ~10°C change on Antarctica (19). Figure 1C shows that fast-feedback climate sensitivity ¾°C per W/m^2 (3°C for doubled CO_2) is a good approximation for the entire period.

Slow feedbacks. Let us consider climate change averaged over a few thousand years – long enough to assure energy balance and minimize effects of ocean thermal response time and climate change leads/lags between hemispheres (20). At such temporal resolution the temperature variations in Fig.1 are global, with high latitude amplification, being present in sea surface temperature derived from ocean sediment cores and polar ice cores (fig S5).

GHG and surface albedo changes are mechanisms causing the large global climate changes in Fig. 1, but they do not initiate these large climate swings. Instead changes of GHGs and sea level (a measure of ice sheet size) lag temperature change by typically several hundred years (6, 7, 21, 22).

GHG and surface albedo changes are positive climate feedbacks. Major glacial-interglacial climate swings are instigated by slow changes of Earth's orbit, especially the tilt of Earth's spin-axis relative to the orbital plane and the precession of the equinoxes that influences the intensity of summer insolation (23, 24). Global radiative forcing due to orbital changes is small, but ice sheet size is affected by changes of geographical and seasonal insolation [e.g., ice melts at both poles when the spin-axis tilt increases, and ice melts at one pole when perihelion, the closest approach to the sun, occurs in late spring, (7)]. Also a warming climate causes net release of GHGs. The most effective GHG feedback is release of CO_2 by the ocean, due partly to temperature dependence of CO_2 solubility but mostly to increased ocean mixing in a warmer climate, which acts to flush out deep ocean CO_2 and alters ocean biological productivity (25).

GHG and surface albedo feedbacks respond and contribute to temperature change caused by any climate forcing, natural or human-made, given sufficient time. The GHG feedback is nearly linear in global temperature during the late Pleistocene (Fig. 7 of 6, 26). Surface albedo feedback increases as Earth becomes colder and the area of ice increases. Climate sensitivity on Pleistocene time scales includes slow feedbacks, and is larger than the Charney sensitivity estimate, because the dominant slow feedbacks are positive. Other feedbacks, e.g., increased weathering as CO_2 increases, may become important on longer geologic time scales.

Paleoclimate data permit evaluation of long-term sensitivity to specified GHG change. We only assume that the area of ice is a function of global temperature. Plotting GHG forcing (7) from ice core data (27) against temperature shows that global climate sensitivity including the slow surface albedo feedback is 1.5°C per W/m^2 or 6°C for doubled CO_2 (Fig. 2), twice as large as the Charney fast-feedback sensitivity.

This long-term climate sensitivity is relevant to GHGs that remain airborne for centuries-to-millennia. GHG amounts will decline if emissions decrease enough, but, on the other hand, if the globe warms much further, carbon cycle models (2) and empirical data (6, 26) find a positive GHG feedback. Amplification of GHGs is moderate if warming is kept within the range of recent interglacial periods (6), but larger warming risks greater release of CH_4 and CO_2 from methane hydrates in tundra and ocean sediments (28).

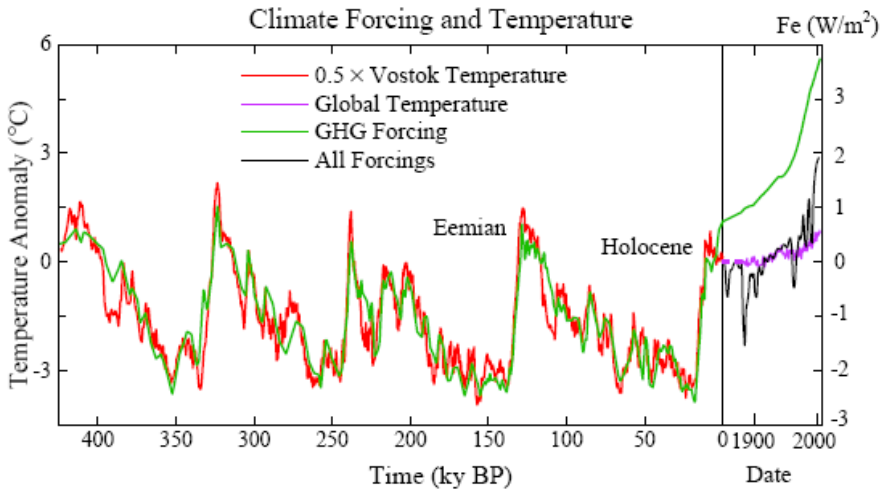

Fig. 2. Global temperature (left scale) and GHG forcing (right scale) due to CO_2, CH_4 and N_2O from the Vostok ice core (16, 27). Ratio of temperature and forcing scales is 1.5°C per W/m^2. The time scale is expanded for the industrial era. Modern forcings include human-made aerosols, volcanic aerosols and solar irradiance (5). GHG forcing zero point is the mean for 10-8 ky BP (Fig. S6). Net climate forcing and modern temperature zero points are at 1850.

Time scales. How long does it take to reach equilibrium temperature? Response is slowed by ocean thermal inertia and the time needed for ice sheets to disintegrate.

Ocean-caused delay is estimated in fig. S7 using a coupled atmosphere-ocean model. One-third of the response occurs in the first few years, in part because of rapid response over land, one-half in ~25 years, three-quarters in 250 years, and nearly full response in a millennium. The ocean-caused delay is a strong (quadratic) function of climate sensitivity and it depends on the rate of mixing of surface water and deep water (29), as discussed in the Supplementary material.

Ice sheet response time is often assumed to be several millennia, based on the broad sweep of paleo sea level change (Fig.1A) and primitive ice sheet models designed to capture that change. However, this long time scale may reflect the slowly changing orbital forcing, rather than inherent inertia, as there is no discernable lag between maximum ice sheet melt rate and local insolation that favors melt (7). Paleo sea level data with high time resolution (30-32) reveal frequent 'suborbital' sea level changes at rates of 1 m/century or more.

Present-day observations of Greenland and Antarctica show increasing surface melt (33), loss of buttressing ice shelves (34), accelerating ice streams (35), and increasing overall mass loss (36). These rapid changes do not occur in existing ice sheet models, which are missing critical physics of ice sheet disintegration (37). Sea level changes of several meters per century occur in the paleoclimate record (30, 31), in response to forcings slower and weaker than the present human-made forcing. It seems likely that large ice sheet response will occur within centuries, if human-made forcings continue to increase. Once ice sheet disintegration is underway, decadal changes of sea level may be substantial.

Warming "in the pipeline". The expanded time scale for the industrial era (Fig. 2) reveals a growing gap between actual global temperature (purple curve) and equilibrium (long-term) temperature response based on the net estimated forcing (black curve). Ocean and ice sheet response times together account for this gap, which is now 2.0°C.

The forcing in Fig. 2 (black curve, Fe scale), when used to drive a global climate model (5), yields global temperature change that agrees closely (fig. 3 in 5) with observations (purple curve, Fig. 2). That climate model, which includes only fast feedbacks, has additional warming of ~0.6°C in the pipeline today because of ocean thermal inertia (5, 8).

The remaining gap between equilibrium temperature for current atmospheric composition and actual global temperature is ~1.4°C. This further 1.4°C warming to come is due to the slow surface albedo feedback, specifically ice sheet disintegration and vegetation change.

One may ask whether the climate system, as the Earth warms from its present 'interglacial' state, still has the capacity to supply slow feedbacks that double the fast-feedback sensitivity. This issue can be addressed by considering longer time scales including periods with no ice.

Cenozoic Era.

Pleistocene atmospheric CO_2 variations occur as a climate feedback, with carbon exchanged among the ocean, atmosphere, soils and biosphere. On longer time scales CO_2 is exchanged between these surface reservoirs and the solid earth, making CO_2 a primary agent of long-term climate change and orbital effects a 'noise' on larger climate swings.

The Cenozoic era, the past 65.5 My, provides a valuable complement to the Pleistocene for exploring climate sensitivity. Cenozoic data on climate and atmospheric composition are not as precise, but larger climate variations occur, including an ice-free planet, thus putting glacial-interglacial changes in a wider perspective.

Oxygen isotopic composition of benthic (deep ocean dwelling) foraminifera shells in a global compilation of ocean sediment cores (24) provides a starting point for analyzing Cenozoic climate change (Fig. 3A). At times with negligible ice sheets, oxygen isotope change, $\delta^{18}O$, provides a direct measure of deep ocean temperature (T_{do}). Thus T_{do} (°C) ~ -4 $\delta^{18}O$ + 12 between 65.5 and 34 My BP.

Rapid increase of $\delta^{18}O$ at about 34 My is associated with glaciation of Antarctica (24, 38) and global cooling, as evidenced by data from North America (39) and Asia (40). From then until the present, ^{18}O in deep ocean foraminifera is affected by both ice volume and T_{do}, lighter ^{16}O evaporating preferentially from the ocean and accumulating in ice sheets. Between 34 My and the last ice age (20 ky) the change of $\delta^{18}O$ was ~ 3‰, change of T_{do} was ~ 6°C (from +5 to -1°C) and ice volume change ~ 180 msl (meters of sea level). Given that a 1.5‰ change of $\delta^{18}O$ is associated with a 6°C T_{do} change, we assign the remaining $\delta^{18}O$ change to ice volume linearly at the rate 60 msl per mil $\delta^{18}O$ change (thus 180 msl for $\delta^{18}O$ between 1.75 and 4.75). Equal division of $\delta^{18}O$ between temperature and sea level yields sea level change in the late Pleistocene in reasonable accord with available sea level data (fig. S8). Subtracting the ice volume portion of $\delta^{18}O$ yields deep ocean temperature T_{do} (°C) = -2 ($\delta^{18}O$ -4.25‰) after 34 My, as in Fig. 3B.

The large (~14°C) Cenozoic temperature change between 50 My and the ice age at 20 ky must have been forced by changes of atmospheric composition. Alternative drives could come from outside (solar irradiance) or the Earth's surface (continental locations). But solar brightness increased ~0.4% in the Cenozoic (41), a linear forcing change of only +1 W/m^2 and of the wrong sign to contribute to the cooling trend. Climate forcing due to continental locations was < 1 W/m^2, because continents 65 My ago were already close to present latitudes (Fig. S9). Opening or closing of oceanic gateways might affect the timing of glaciation, but it would not provide the climate forcing needed for global cooling.

CO_2 concentration, in contrast, varied from ~180 ppm in glacial times to 1500 ± 500 ppm in the early Cenozoic (42). This change is a forcing of more than 10 W/m^2 (Table 1 in 15), an order of magnitude larger than other known forcings. CH_4 and N_2O, positively correlated with CO_2 and global temperature in the period with accurate data (ice cores), likely increase the total GHG forcing, but their forcings are much smaller than that of CO_2 (43, 44).

Cenozoic carbon cycle. Solid Earth sources and sinks of CO_2 are generally not balanced (45). CO_2 is removed from surface reservoirs by: (1) chemical weathering of rocks with deposition of carbonates on the ocean floor, and (2) burial of organic matter; weathering is the

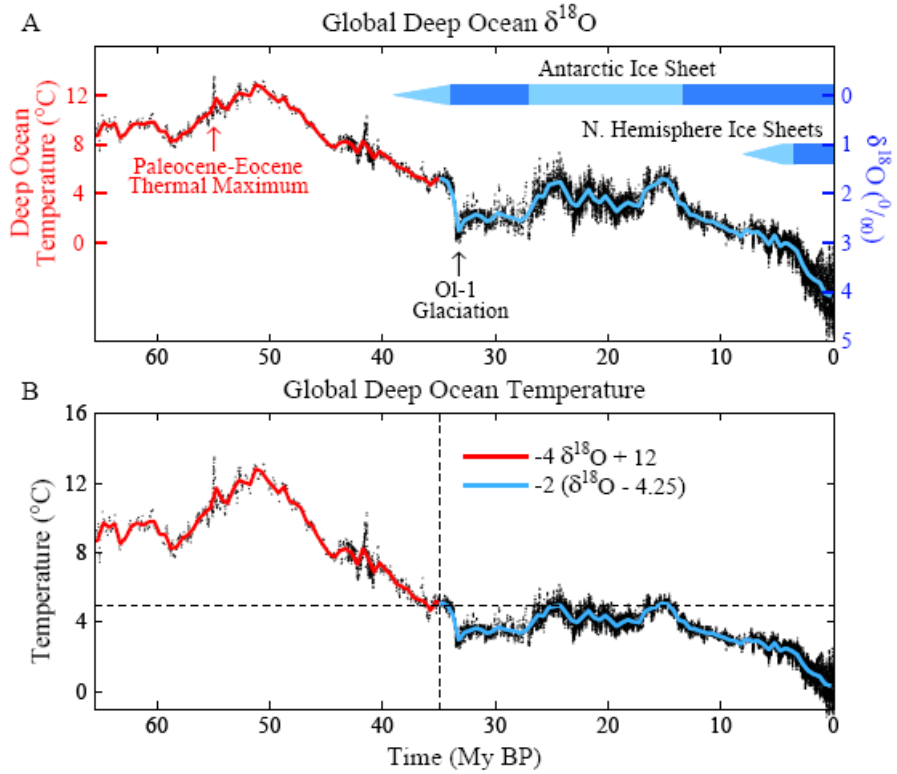

Fig. 3. Global deep ocean (A) $\delta^{18}O$ (24) and (B) temperature. Black curve is 5-point running mean of $\delta^{18}O$ original temporal resolution, while red and blue curves have 500 ky resolution.

dominant process (46). CO_2 returns primarily via metamorphism and volcanic outgassing where carbonate-rich oceanic crust is subducted beneath moving continental plates.

Burial and outgassing of CO_2 are each typically 2-4×10^{12} mol C/year (46, 47). An imbalance of 2×10^{12} mol C/year, confined to the atmosphere, is ~0.01 ppm/year, but as CO_2 is distributed among surface reservoirs, it is only ~0.0001 ppm/year. This is a negligible rate compared to the present human-made atmospheric CO_2 increase of ~2 ppm/year, yet over a million years this small crustal imbalance alters atmospheric CO_2 by 100 ppm.

Between 60 and 50 My ago India moved north rapidly, 18-20 cm/year (48), through a region that long had been a depocenter for carbonate and organic sediments. Subduction of carbonate-rich crust was surely a source of CO_2 outgassing and a prime cause of global warming, which peaked 50 My ago (Fig. 3b) with the Indo-Asian collision that initiated uplift of the Himalayas and Tibetan Plateau that subsequently increased drawdown of atmospheric CO_2 by enhanced weathering (49). Since then the Indian and Atlantic Oceans have been the major depocenters for carbon, with subduction of carbon-rich crust limited largely to small regions near Indonesia and Central America (46).

Thus atmospheric CO_2 declined in the past 50 My (42) and climate cooled (Fig. 3B) leading to Antarctic glaciation by ~34 My. Antarctica has remained glaciated ever since, although glaciation may have reversed temporarily, e.g., ~26 My ago, perhaps due to negative feedback of reduced weathering (50).

Knowledge of Cenozoic CO_2 is limited to imprecise proxy measures except for recent ice core data. However, the proxy data indicate that CO_2 was ~1000-2000 ppm in the early Cenozoic and <500 ppm in the last 20 My (2, 42).

Cenozoic forcing and CO_2. The entire Cenozoic climate forcing history (Fig. 4A) is implied by the temperature reconstruction (Fig. 3B), assuming a fast-feedback sensitivity of ¾°C per W/m^2. Subtracting the solar and surface albedo forcings (Fig. 4B), the latter from Eq. S2 with ice sheet area vs time from $\delta^{18}O$, we obtain the GHG forcing history Fig. 4C).

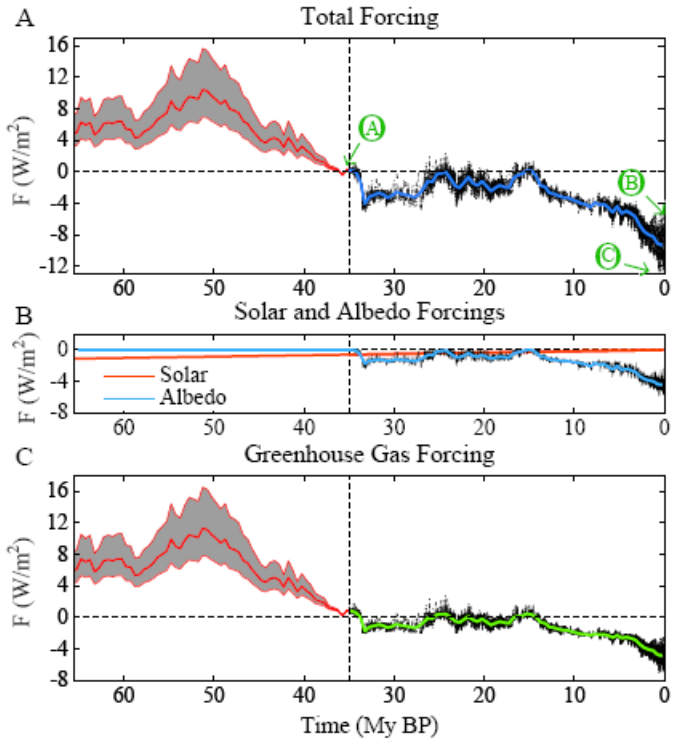

Fig. 4. (A) Total climate forcing, (B) solar and surface albedo forcings, and (C) GHG forcing in the Cenozoic, based on T_{do} history of Fig. 3B and assumed fast-feedback climate sensitivity ¾°C per W/m^2. Ratio of T_s change and T_{do} change is assumed to be near unity in the minimal ice world between 65 and 35 My, but the gray area allows for 50% uncertainty in the ratio. In the later era with large ice sheets we take T_s/T_{do} = 1.5, in accord with Pleistocene data.

We hinge our calculations 35 My ago for several reasons. Between 65 and 35 My ago there was little ice on the planet, so climate sensitivity is defined mainly by fast feedbacks. Second, we want to estimate the CO_2 amount that precipitated Antarctic glaciation. Finally, the relation between global surface air temperature change (ΔT_s) and deep ocean temperature change (ΔT_{do}) differs for ice-free and glaciated worlds.

In the ice-free world (65-35 My) we take $\Delta T_s \sim \Delta T_{do}$ with generous (50%) uncertainty, as climate models show that global temperature change is tied closely to ocean temperature change (51). In the glaciated world ΔT_{do} is limited by the freezing point in the deep ocean. ΔT_s between the last ice age (20 ky) and the present interglacial period (~5°C) was ~1.5 times larger than ΔT_{do}. In fig. S5 we show that this relationship fits well throughout the period of ice core data.

If we specify CO_2 at 35 My, the GHG forcing defines CO_2 at other times, assuming CO_2 provides 75% of the GHG forcing, as in the late Pleistocene. CO_2 ~400-450 ppm at 35 My keeps CO_2 in the range of early Cenozoic proxies (Fig. 5A) and yields a good fit to the amplitude and mean CO_2 amount in the late Pleistocene (Fig. 5B). A ~500 ppm CO_2 threshold for Antarctic glaciation was previously inferred from proxy CO_2 data and a carbon cycle model (52).

Individual CO_2 proxies (Fig. S10) clarify limitations due to scatter among the measurements. Low CO_2 of some early Cenozoic proxies suggests higher climate sensitivity. However, in general the sensitivities inferred from the Cenozoic and Phanerozoic (53, 54, 55) agree well with our analysis, if we account for the ways in which sensitivity is defined and the periods emphasized in each empirical derivation (Table S1).

A CO_2 estimate of ~425 ppm at 35 My (Fig. 5) serves as a prediction to compare with new data on CO_2 amount. Model uncertainties (Fig. S10) include possible changes of non-CO_2 GHGs and the relation of ΔT_s to ΔT_{do}. The model fails to account for cooling in the past 15 My if CO_2 increased, as most proxies suggest (Fig. S10). Changing ocean currents, such as the closing of the Isthmus of Panama, may have contributed to climate evolution, but models find little effect

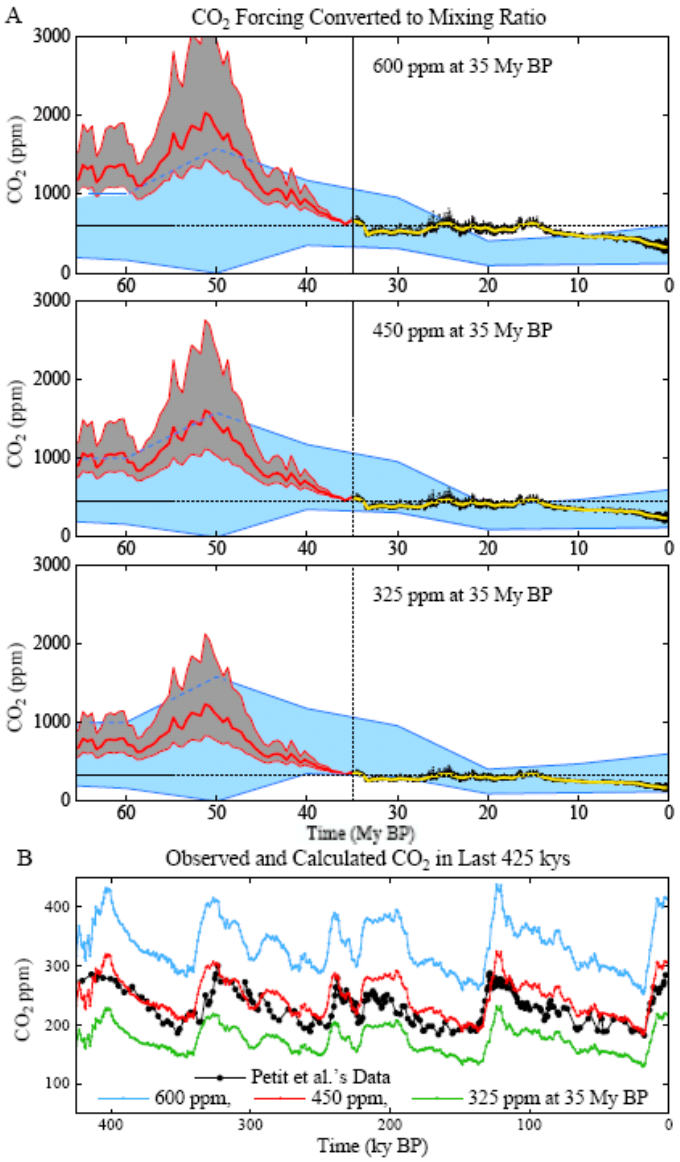

Fig. 5. (A) Simulated CO_2 amounts in the Cenozoic for three choices of CO_2 amount at 35 My (temporal resolution of black and colored curves as in Fig. 3; blue region: multiple CO_2 proxy data; gray region allows 50 percent uncertainty in ratio of global surface and deep ocean temperatures). (B) Expanded view of late Pleistocene, including precise ice core CO_2 measurements (black curve).

on temperature (56). Non-CO_2 GHGs also could have played a role, because little forcing would have been needed to cause cooling due to the magnitude of late Cenozoic albedo feedback.

Implications. We infer from Cenozoic data that CO_2 was the dominant Cenozoic forcing, that CO_2 was ~350-500 ppm when Antarctica glaciated, and that glaciation is reversible. Together these inferences have profound implications.

Consider three points marked in Fig. 4: point A at 35 My, just before Antarctica glaciated; point B at recent interglacial periods; point C at the depth of recent ice ages. Point B is half way between points A and C in global temperature (Fig. 3B) and climate forcings (Fig. 4). For example, the climate forcing for CO_2 change from 180 to 285 ppm is 2.6 W/m^2 and further change from 285 to 450 ppm is 2.7 W/m^2.

Thus equilibrium climate sensitivity that includes slow feedbacks is about 1.5°C per W/m^2 or 6°C for doubled CO_2 between today and an ice-free world, the same as between today and the last ice age. Evidently amplification provided by loss of Greenland and Antarctic ice and spread of flora over the vast high-latitude land area in the Northern Hemisphere, in response to positive forcing, is comparable to amplification provided by the Laurentide and other ice sheets, in response to negative forcing.

Anthropocene Era.

Human-made global climate forcings now prevail over natural forcings (Fig. 2). Earth may have entered the Anthropocene era (57, 58) 6-8 ky ago (59), but the net human-made forcing was small, perhaps slightly negative (7), prior to the industrial era. GHG forcing overwhelmed natural and negative human-made forcings only in the past quarter century (Fig. 2).

Human-made climate change is delayed by ocean (fig. S7) and ice sheet response times. Warming 'in the pipeline', mostly attributable to slow feedbacks, is now about 2°C (Fig. 2). No additional forcing is required to raise global temperature to at least the level of the Pliocene, 2-3 million years ago, a degree of warming that would surely yield 'dangerous' climate impacts (5).

Tipping points. Realization that today's climate is far out of equilibrium with current climate forcings raises the specter of 'tipping points', the concept that climate can reach a point where, without additional forcing, rapid changes proceed practically out of our control (2, 7, 60). Arctic sea ice and the West Antarctic Ice Sheet are examples of potential tipping points. Arctic sea ice loss is magnified by the positive feedback of increased absorption of sunlight as global warming initiates sea ice retreat (61). West Antarctic ice loss can be accelerated by several feedbacks, once ice loss is substantial (37).

We define: (1) the *tipping level*, the global climate forcing that, if long maintained, gives rise to a specific consequence, and (2) the *point of no return*, a climate state beyond which the consequence is inevitable, even if climate forcings are reduced. A point of no return can be avoided, even if the tipping level is temporarily exceeded. Ocean and ice sheet inertia permit overshoot, provided the climate forcing is returned below the tipping level before initiating irreversible dynamic change.

Points of no return are inherently difficult to define, because the dynamical problems are nonlinear. Existing models are more lethargic than the real world for phenomena now unfolding, including changes of sea ice (62), ice streams (63), ice shelves (64), and expansion of the subtropics (65, 66).

The tipping level is easier to assess, because the paleoclimate equilibrium response to known climate forcing is relevant. The tipping level is a measure of the long-term climate forcing that humanity must aim to stay beneath to avoid large climate impacts. The tipping level does not define the magnitude or period of tolerable overshoot. However, if overshoot is in place for centuries, the thermal perturbation will so penetrate the ocean (10) that recovery without dramatic effects, such as ice sheet disintegration, becomes unlikely.

Target CO_2. GHGs other than CO_2 cause climate forcing comparable to that of CO_2 (2, 6), but growth of non-CO_2 GHGs is falling below IPCC (2) scenarios and the GHG climate forcing change is determined mainly by CO_2 (67). Net human-made forcing is comparable to the CO_2 forcing, as non-CO_2 GHGs tend to offset negative aerosol forcing (2, 5).

Thus we take future CO_2 change as approximating the net human-made forcing change, with two caveats. First, special effort to reduce non-CO_2 GHGs could alleviate the CO_2 requirement, allowing up to about +25 ppm CO_2 for the same climate effect, while resurgent growth of non-CO_2 GHGs could reduce allowed CO_2 a similar amount (6). Second, reduction of human-made aerosols, which have a net cooling effect, could force stricter GHG requirements. However, an emphasis on reducing black soot could largely off-set reductions of high albedo aerosols (18).

We define a target CO_2 level by considering several specific climate impacts:

Civilization is adapted to climate zones of the Holocene. Theory and models indicate that subtropical regions expand poleward with global warming (2, 65). Data reveal a 4-degree latitudinal shift already (66), larger than model predictions, yielding increased aridity in southern

United States, the Mediterranean region, Australia and parts of Africa. Impacts of this climate shift (69) support the conclusion that 385 ppm CO_2 is already deleterious.

Alpine glaciers are in near-global retreat (69, 70). After a flush of fresh water, glacier loss foretells long summers of frequently dry rivers, including rivers originating in the Himalayas, Andes and Rocky Mountains that now supply water to hundreds of millions of people. Present glacier retreat, and warming in the pipeline, indicate that 385 ppm CO_2 is already a threat.

Equilibrium sea level rise for today's 385 ppm CO_2 is at least several meters, judging from paleoclimate history (31, 17, 30). Accelerating mass losses from Greenland (71) and West Antarctica (72) heighten concerns about ice sheet stability. An initial CO_2 target of 350 ppm, to be reassessed as the effect on ice sheet mass balance is observed, is suggested.

Stabilization of Arctic sea ice cover requires, to first approximation, restoration of planetary energy balance. Climate models driven by known forcings yield a present planetary energy imbalance of +0.5-1 W/m^2 (5), a result supported by observed increasing ocean heat content (73). CO_2 amount must be reduced to 325-355 ppm to increase outgoing flux 0.5-1 W/m^2, if other forcings are unchanged. A further reduced flux, by ~0.5 W/m^2, and thus CO_2 ~300-325 ppm, may be needed to restore sea ice to its area of 25 years ago.

Coral reefs are suffering from multiple stresses, with ocean acidification and ocean warming principal among them (74). Given additional warming 'in-the-pipeline', 385 ppm CO_2 is already deleterious. A 300-350 ppm CO_2 target would significantly relieve both of these stresses.

CO_2 scenarios. A large fraction of fossil fuel CO_2 emissions stays in the air a long time, one-quarter remaining airborne for several centuries (5, 75-77). Thus moderate delay of fossil fuel use will not appreciably reduce long-term human-made climate change. Preservation of climate requires that most remaining fossil fuel carbon is never emitted to the atmosphere.

Coal is the largest reservoir of conventional fossil fuels (fig. S12), exceeding combined reserves of oil and gas (2, 77). The only realistic way to sharply curtail CO_2 emissions is to phase out coal use except where CO_2 is captured and sequestered.

Phase-out of coal emissions by 2030 (Fig. 6) keeps maximum CO_2 close to 400 ppm, depending on oil and gas reserves and reserve growth. IPCC reserves assume that half of readily extractable oil has already been used (figs. 6, S12). EIA (78) estimates (fig. S12) have larger reserves and reserve growth. Even if EIA estimates are accurate, the IPCC case remains valid if the most difficult to extract oil and gas is left in the ground, via a rising price on carbon emissions that discourages remote exploration and environmental regulations that place some areas off-limit. If IPCC gas reserves (fig. S12) are underestimated, the IPCC case in Fig. 6 remains valid if added gas reserves are used at facilities where CO_2 is captured.

However, even with phase-out of coal emissions and assuming IPCC oil and gas reserves, CO_2 would remain above 350 ppm for more than two centuries. Ongoing Arctic and ice sheet changes, examples of rapid paleoclimate change, and other criteria cited above all drive us to consider scenarios that bring CO_2 more rapidly back to 350 ppm or less.

Policy relevance. Desire to reduce airborne CO_2 raises the question of whether CO_2 could be drawn from the air artificially. There are no large-scale technologies for CO_2 air capture now, but with strong research and development support and industrial-scale pilot projects sustained over decades it may be possible to achieve costs ~$200/tC (79) or perhaps less (80). At $100/tC, the cost of removing 50 ppm of CO_2 is ~$10 trillion.

Improved agricultural and forestry practices offer a more natural way to draw down CO_2. Deforestation contributed a net emission of 60±30 ppm over the past few hundred years, of which ~20 ppm CO_2 remains in the air today (2, 81, figs S12, S14). Reforestation could absorb a significant fraction of the 60±30 ppm net deforestation emission.

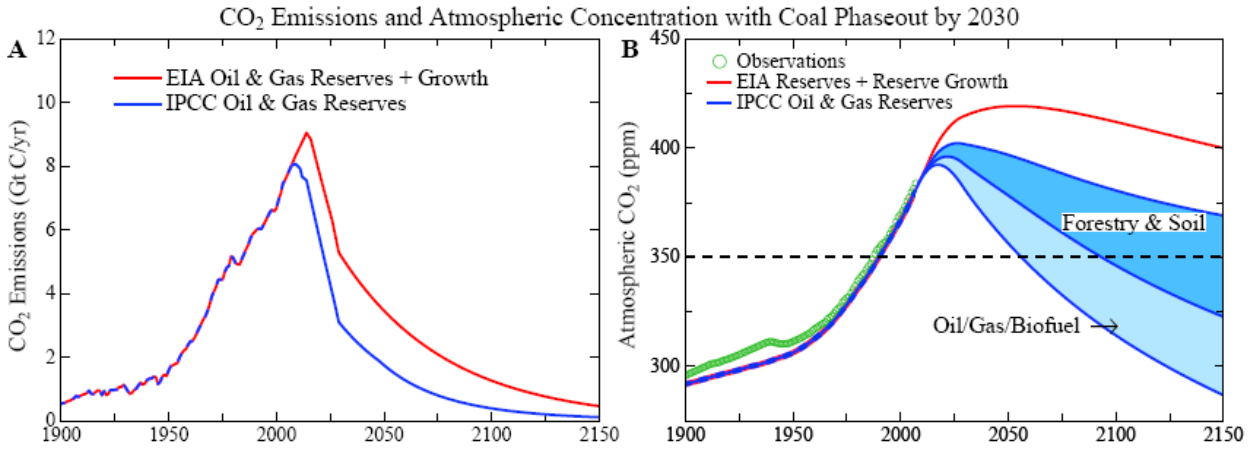

Fig. 6. (A) Fossil fuel CO_2 emissions with coal phase-out by 2030 based on IPCC (2) and EIA (78) estimated fossil fuel reserves. (B) Resulting atmospheric CO_2 based on use of a dynamic-sink pulse response function representation of the Bern carbon cycle model (76, 77).

Carbon sequestration in soil also has significant potential. Biochar, produced in pyrolysis of residues from crops, forestry, and animal wastes, can be used to restore soil fertility while storing carbon for centuries to millennia (82). Biochar helps soil retain nutrients and fertilizers, reducing emissions of GHGs such as N_2O (83). Replacing slash-and-burn agriculture with slash-and-char and use of agricultural and forestry wastes for biochar production could provide a CO_2 drawdown of ~8 ppm in half a century (83).

In Supplementary Material we define a forest/soil drawdown scenario that reaches 50 ppm by 2150 (Fig. 6B). This scenario returns CO_2 below 350 ppm late this century, after about 100 years above that level.

More rapid drawdown could be provided by CO_2 capture at power plants fueled by gas and biofuels (84). Low-input high-diversity biofuels grown on degraded or marginal lands, with associated biochar production, could accelerate CO_2 drawdown, but the nature of a biofuel approach must be carefully designed (83, 85-87).

A rising price on carbon emissions and payment for carbon sequestration is surely needed to make drawdown of airborne CO_2 a reality. A 50 ppm drawdown via agricultural and forestry practices seems plausible. But if most of the CO_2 in coal is put into the air, no such "natural" drawdown of CO_2 to 350 ppm is feasible. Indeed, if the world continues on a business-as-usual path for even another decade without initiating phase-out of unconstrained coal use, prospects for avoiding a dangerously large, extended overshoot of the 350 ppm level will be dim.

Summary.

Humanity today, collectively, must face the uncomfortable fact that industrial civilization itself has become the principal driver of global climate. If we stay our present course, using fossil fuels to feed a growing appetite for energy-intensive life styles, we will soon leave the climate of the Holocene, the world of prior human history. The eventual response to doubling pre-industrial atmospheric CO_2 likely would be a nearly ice-free planet.

Humanity's task of moderating human-caused global climate change is urgent. Ocean and ice sheet inertias provide a buffer delaying full response by centuries, but there is a danger that human-made forcings could drive the climate system beyond tipping points such that change proceeds out of our control. The time available to reduce the human-made forcing is uncertain, because models of the global system and critical components such as ice sheets are inadequate.

However, climate response time is surely less than the atmospheric lifetime of the human-caused perturbation of CO_2. Thus remaining fossil fuel reserves should not be exploited without a plan for retrieval and disposal of resulting atmospheric CO_2.

Paleoclimate evidence and ongoing global changes imply that today's CO_2, about 385 ppm, is already too high to maintain the climate to which humanity, wildlife, and the rest of the biosphere are adapted. Realization that we must reduce the current CO_2 amount has a bright side: effects that had begun to seem inevitable, including impacts of ocean acidification, loss of fresh water supplies, and shifting of climatic zones, may be averted by the necessity of finding an energy course beyond fossil fuels sooner than would otherwise have occurred.

We suggest an initial objective of reducing atmospheric CO_2 to 350 ppm, with the target to be adjusted as scientific understanding and empirical evidence of climate effects accumulate. Limited opportunities for reduction of non-CO_2 human-caused forcings are important to pursue but do not alter the initial 350 ppm CO_2 target. This target must be pursued on a timescale of decades, as paleoclimate and ongoing changes, and the ocean response time, suggest that it would be foolhardy to allow CO_2 to stay in the dangerous zone for centuries.

A practical global strategy almost surely requires a rising global price on CO_2 emissions and phase-out of coal use except for cases where the CO_2 is captured and sequestered. The carbon price should eliminate use of unconventional fossil fuels, unless, as is unlikely, the CO_2 can be captured. A reward system for improved agricultural and forestry practices that sequester carbon could remove the current CO_2 overshoot. With simultaneous policies to reduce non-CO_2 greenhouse gases, it appears still feasible to avert catastrophic climate change.

Present policies, with continued construction of coal-fired power plants without CO_2 capture, suggest that decision-makers do not appreciate the gravity of the situation. We must begin to move now toward the era beyond fossil fuels. Continued growth of greenhouse gas emissions, for just another decade, practically eliminates the possibility of near-term return of atmospheric composition beneath the tipping level for catastrophic effects.

The most difficult task, phase-out over the next 20-25 years of coal use that does not capture CO_2, is herculean, yet feasible when compared with the efforts that went into World War II. The stakes, for all life on the planet, surpass those of any previous crisis. The greatest danger is continued ignorance and denial, which could make tragic consequences unavoidable.

References and Notes

1. Framework Convention on Climate Change, United Nations, http://www.unfccc.int/, (1992).
2. Intergovernmental Panel on Climate Change (IPCC), *Climate Change 2007*, S. Solomon et al., Eds. (Cambridge Univ. Press, New York, 2007).
3. M.D. Mastrandrea, S.H. Schneider, *Science* **304**, 571 (2004).
4. European Council, Climate change strategies (2005) http://register.consilium.europa.eu/pdf/en/05/st07/st07242.en05.pdf
5. J. Hansen et al., *Atmos. Chem. Phys.* **7**, 2287 (2007).
6. J. Hansen, M. Sato, *Proc. Natl. Acad. Sci.* **101**, 16109 (2004).
7. J. Hansen *et al., Phil. Trans. Roy. Soc. A* **365**, 1925 (2007).
8. J. Hansen *et al., Science* **308**, 1431 (2005).
9. L.D.D. Harvey, *Clim. Change* **82**, 1 (2007).
10. H.D. Matthews, K. Caldeira, *Geophys. Res. Lett.* **35**, L04705 (2008).
11. J. Hansen *et al., J. Geophys. Res.* **110**, D18104 (2005).
12. J. Charney, *Carbon Dioxide and Climate: A Scientific Assessment* (Natl. Acad. Sci. Press, Washington, D.C., 1979).
13. J. Hansen *et al., Am. Geophys. Union Geophys.* Mono. Ser. **29**, 130 (1984).
14. P. Braconnot *et al., Clim. Past* **3**, 261 (2007).

15. I. Farrera *et al., Clim. Dyn.* **15**, 823 (1999).
16. J.R. Petit *et al., Nature* **399**, 429 (1999).
17. M. Siddall *et al., Nature* **423**, 853 (2003).
18. J. Hansen *et al., Proc. Natl. Acad. Sci.* **97**, 9875 (2000).
19. V. Masson-Delmotte *et al., Clim. Dyn.* **26**, 513 (2006).
20. EPICA community, *Nature* **444**, 195 (2006).
21. N. Caillon *et al., Science* **299**, 1728 (2003).
22. M. Mudelsee, *Quat. Sci. Rev.* **20**, 583 (2001).
23. J.D. Hays, *et al., Science* **194**, 1121 (1976).
24. J. Zachos, *Science* **292**, 686 (2001).
25. P. Kohler, H. Fischer, *Clim. Past* **2**, 57-78 (2006).
26. U. Siegenthaler *et al., Science* **310**, 1313 (2005).
27. F. Vimeux, K.M. Cuffey, J. Jouzel, *Earth Planet. Sci. Lett.* **203**, 829 (2002).
28. D. Archer, *Biogeosci.* **4**, 521 (2007).
29. J. Hansen *et al., Science* **229**, 857 (1985).
30. W.G. Thompson, S.L. Goldstein, *Science* **308**, 401 (2005).
31. P.J. Hearty *et al., Quat. Sci. Rev.* **26**, 2090 (2007).
32. E.J. Rohling *et al, Nature Geosci.* **1**, 38 (2008).
33. M. Tedesco, *Geophys. Res. Lett.* **34**, L02504 (2007).
34. E. Rignot, S.S. Jacobs, *Science* **296**, 2020 (2002).
35. H.J. Zwally *et al., Science* **297**, 218 (2002).
36. J.L. Chen, *et al., Science* **313**, 1958 (2006).
37. J. Hansen, *Clim. Change* **68**, 269 (2005).
38. R.M.DeConto, D. Pollard, *Nature* **421**, 245 (2003).
39. A. Zanazzi *et al., Nature* **445**, 639 (2007).
40. G. Dupont-Nivet *et al., Nature* **445**, 635 (2007).
41. L.J. Sackmann *et al., Astrophys. J.* **418**, 457 (1993).
42. M. Pagani *et al., Science* **309**, 600 (2005).
43. O. Bartdorff *et al., Global Biogeochem. Cycles* **22**, GB1008 (2008).
44. D. Beerling *et al., Am. J. Sci.*, in press (2008).
45. J.M. Edmond, Y. Huh, *Earth Planet. Sci. Lett.* **216**, 125 (2003).
46. R.A. Berner, *The Phanerozoic Carbon Cycle: CO2 and O2* (Oxford Univ. Press, New York, 2004).
47. H. Staudigel *et al., Geochim. Cosmochim. Acta* **53**, 3091 (1989).
48. P. Kumar *et al., Nature* **449**, 894 (2007).
49. M.E. Raymo and W.F. Ruddiman, *Nature* **359**, 117 (1992).
50. C.H. Lear *et al., Paleocean.* **19**, PA4015 (2004).
51. M.M. Joshi, *et al., Clim. Dyn.* **30**, 455 (2008).
52. D.L. Royer, *Geochim. Cosmochim. Acta* **70**, 5665 (2006).
53. D.L. Royer *et al., Nature* **446**, 530 (2007).
54. J.A. Higgins, D.P. Schrag, *Earth Plan. Sci. Lett.* **245**, 523 (2006).
55. M. Pagani, *et al., Science* **314**, 1556 (2006).
56. D.J. Lunt *et al. Clim. Dyn.* **30**, 1 (2008).
57. P.J. Crutzen, *Global Change Newsletter* **41**, 12 (2000).
58. J. Zalasiewicz *et al., GSA Today* **18**, 4 (2008).
59. W.F. Ruddiman, *Clim. Change* **61**, 261 (2003).
60. T.M. Lenton *et al., Proc. Natl. Acad. Sci.* **105**, 1786 (2008).
61. R.W. Lindsay, J. Zhang, *J. Climate* **18**, 4879 (2005).
62. J. Stroeve et al., EOS Trans. Amer. Geophys. Union 89, 13 (2008).
63. I.M. Howat *et al., Science* **315**, 1559 (2007).
64. E. Rignot, S.S. Jacobs, *Science* **296**, 2020 (2002).
65. I.M. Held, B.J. Soden, *J. Climate* **19**, 5686 (2006).
66. D.J. Seidel, W.J. Randel, *J. Geophys. Res.* **111**, D21101 (2006).

67. J. Hansen, M. Sato, *Open Environ. J.* (submitted).
69. Intergovernmental Panel on Climate Change (IPCC), *Impacts, Adaptation and* V*ulnerability*, M. Parry *et al.*, Eds. (Cambridge Univ. Press, New York, 2007).
70. T.P. Barnett *et al., Nature* **438**, 303 (2005).
71. K. Steffen*, et al*., Chap. 2 in *Abrupt Climate Change*, U.S. Climate Change Science Program, SAP 3.4 (in press).
72. E. Rignot *et al., Nature Geoscience*, doi:10.1038/ngeo102 (2008).
73. S. Levitus *et al., Geophys. Res. Lett.* **32**, L02604 (2005).
74. R. Stone, *Science* **316**, 678 (2007).
75. D. Archer, *J. Geophys. Res.* **110**, C09S05 (2005).
76. F. Joos, et al., *Tellus* **48B**, 397 (1996).
77. P.A. Kharecha, J.E. Hansen, *Global Biogeo. Cycles* (in press).
78. Energy Information Administration (EIA), U.S. DOE, *International Energy Outlook 2006*, http://www.eia.doe.gov/oiaf/archive/ieo06/index.html (2006).
79. D.W. Keith, *et al., Clim. Change* **74**, 17 (2006).
80. K. Lackner, *Science* **300**, 1677 (2003)
81. R.A. Houghton, *Tellus* **55B**, 378 (2003).
82. J. Lehmann, *Nature* **447**, 143 (2007).
83. J. Lehmann, *et al., Mitiga. Adap. Strat. Glob. Chan.* **11**, 403 (2006).
84. J. Hansen, Congressional Testimony, http://arxiv.org/abs/0706.3720v1 (2007).
85. D. Tilman, J. Hill, C. Lehman, Science **314**, 1598 (2006).
86. J. Fargione, *et al., Science* **319**, 1235 (2008).
87. T. Searchinger, *et al., Science* **319**, 1238 (2008).
88. We thank H. Harvey, G. Lenfest, the Rockefeller Foundation, and NASA program managers D. Anderson and J. Kaye for research support, S. Baum, P. Essunger, K. Farnish, Q. Fu, L.D. Harvey, I. Horovitz, C. Kutscher, J. Leventhal, C. McGrath, T. Noerpel, P. Read, J. Romm, D. Sanborn, S. Schwartz, K. Ward and S. Weart for comments on a draft manuscript, and NOAA Earth System Research Laboratory for data.

Supporting Online Material

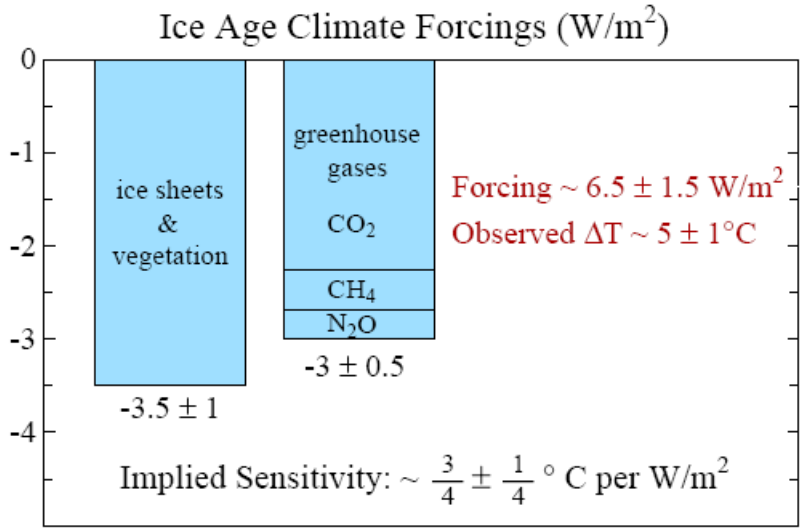

Fig. S1. Climate forcings during ice age 20 ky BP, relative to the present (pre-industrial) interglacial period.

Ice age climate forcings. Figure S1 shows the climate forcings during the depth of the last ice age, 20 ky BP, relative to the Holocene (13). The largest contribution to the uncertainty in the calculated 3.5 W/m^2 forcing due to surface changes (ice sheet area, vegetation distribution, shoreline movements) is due to uncertainty in the ice sheet sizes (13, S1). Formulae (18) for the GHG forcings yield 2.25 W/m^2 for CO_2 (185 ppm → 275 ppm), 0.43 W/m^2 for CH_4 (350 → 675 ppb) and 0.32 W/m^2 for N_2O (200 → 270 ppb). The CH_4 forcing includes a factor 1.4 to account for indirect effects of CH_4 on tropospheric ozone and stratospheric water vapor (11).

The climate sensitivity inferred from the ice age climate change (~¾°C per W/m^2) includes only fast feedbacks, such as water vapor, clouds, aerosols (including dust) and sea ice. Ice sheet size and greenhouse gas amounts are specified boundary conditions in this derivation of the fast-feedback climate sensitivity.

It is permissible to, alternatively, specify aerosol changes as part of the forcing and thus derive a climate sensitivity that excludes the effect of aerosol feedbacks. That approach was used in the initial empirical derivation of climate sensitivity from Pleistocene climate change (13). The difficulty with that approach is that, unlike long-lived GHGs, aerosols are distributed heterogeneously, so it is difficult to specify aerosol changes accurately. Also the forcing is a sensitive function of aerosol single scatter albedo, which is also not well measured, and the vertical distribution of aerosols in the atmosphere. Further, the aerosol indirect effect on clouds also depends upon all of these poorly known aerosol properties.

One recent study (S2) specified an arbitrary glacial-interglacial aerosol forcing slightly larger than the GHG glacial-interglacial forcing. As a result, because temperature, GHGs, and aerosol amount, overall, are positively correlated in glacial-interglacial changes, this study inferred a climate sensitivity of only ~2°C for doubled CO_2. This study used the correlation of aerosol and temperature in the Vostok ice core at two specific times to infer an aerosol forcing for a given aerosol amount. The conclusions of the study are immediately falsified by considering the full Vostok aerosol record (Fig. 2, 16), which reveals numerous large aerosol fluctuations without any corresponding temperature change. In contrast, the role of GHGs in climate change is confirmed when this same check is made for GHGs (Fig. 2), and the fast-feedback climate sensitivity of 3°C for doubled CO_2 is confirmed (Fig. 1).

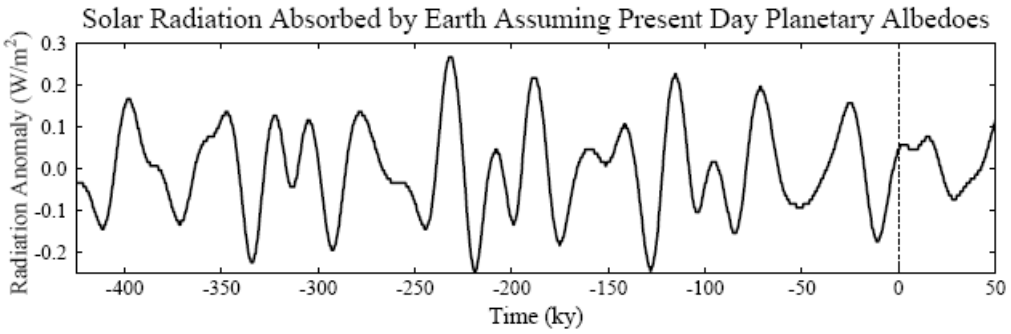

Fig. S2. Annual-mean global-mean perturbation of the amount of solar radiation absorbed by the Earth, calculated by assuming present-day seasonal and geographical distribution of albedo.

All the problems associated with imprecise knowledge of aerosol properties become moot if, as is appropriate, aerosols are included in the fast feedback category. Indeed, soil dust, sea salt, dimethylsulfide, and other aerosols are expected to vary (in regional, inhomogeneous ways) as climate changes. The effect of these aerosol changes is fully included in the observed global temperature change. The climate sensitivity that we derive in Fig. S1 includes the aerosol effect accurately, because both the climate forcings and the global climate response are known. The indirect effect of aerosol change on clouds is, of course, also included precisely.

Earth orbital (Milankovitch) climate forcing. Figure S2 shows the perturbation of solar radiation absorbed by the Earth due to changes in Earth orbital elements, i.e., the tilt of the Earth's spin axis relative to the orbital plane, the eccentricity of the Earth's orbit, and the time of year at which the Earth is closest to the sun (precession of equinoxes). This perturbation is calculated assuming fixed (present day) seasonal and geographical distribution of planetary albedo. It measures the global forcing that instigates the glacial-interglacial climate changes.

This weak forcing is negligible, per se, on global-mean annual-mean basis. However, regional seasonal insolation perturbations are as much as several tens of W/m^2. These insolation perturbations instigate ice sheet and GHG changes, slow feedbacks, which amplify the global annual-mean orbital forcing.

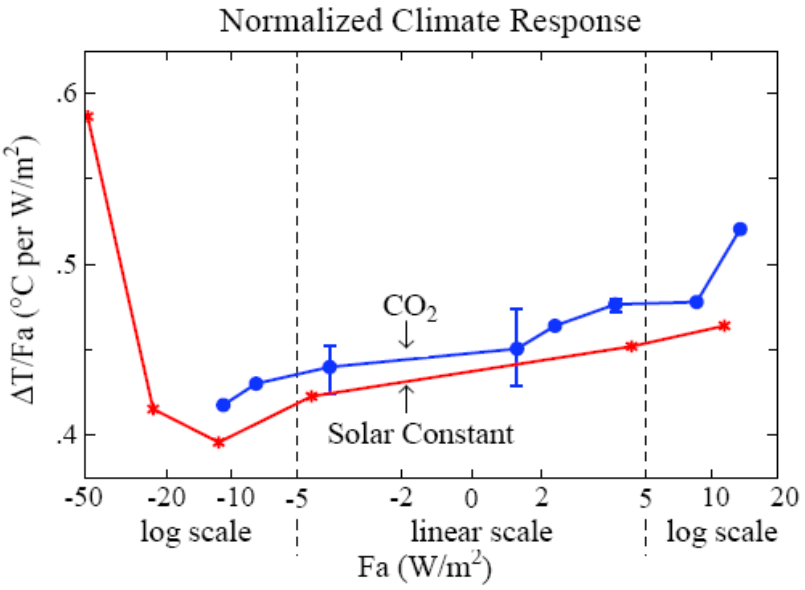

Fig. S3. Global surface air temperature change (11) after 100 years (mean of years 81-120) in simulations with the Goddard Institute for Space Studies (GISS) modelE (S3, 5) as a function of climate forcing for changes of solar irradiance and atmospheric CO_2. Fa is the standard adjusted climate forcing (11). Results here are extracted from Fig. 25(a) of (11).

Climate response function. Figure S3 shows that climate forcings of the order of 20-50 W/m^2 are needed to approach either the runaway snowball-Earth feedback or the runaway greenhouse effect, if only the Charney fast feedbacks are included. However, the negative forcing required to approach snowball-Earth is reduced by amplifying slow feedbacks, especially increasing ice sheet area. Indeed, the real-world Earth has experienced snowball conditions (S4), or at least a 'slushball' state (S5), on at least two occasions, the most recent ~640 My BP, aided by reduced solar irradiance (41) and favorable continental locations. The mechanism that allowed Earth to escape from the snowball state was probably the reduced weathering in a glaciated world, which allowed volcanic CO_2 to accumulate in the atmosphere (S4).

It would , of course, be interesting to extend the simulations of Fig. S3 to both smaller and larger forcings. The reason that the curves in Fig. 2 terminate is that the climate model "bombed" at the next increment of forcing due to failure of one or more of the parameterizations of physical processes in the model when extreme conditions are approached. The accuracy of the representations at extreme temperatures must be improved before the model can be used to simulate well transitions to snowball Earth or the runaway greenhouse effect.

Ice sheet albedo. In the present paper we take the surface area covered by an ice sheet to be proportional to the 4/5 power of the volume of the ice sheet, based on ice sheet modeling of one of us (VM-D). We extend the formulation all the way to zero ice on the planet, with separate terms for each hemisphere. At 20 ky ago, when the ice sheets were at or near their maximum size in the Cenozoic era, the forcing by the Northern Hemisphere ice sheet was -3.5 W/m^2 and the forcing by the Southern Hemisphere ice sheet was -2 W/m^2, relative to the ice-free planet (11). It is assumed that the first 60 m of sea level fall went entirely into growth of the Southern Hemisphere ice sheet. The water from further sea level fall is divided proportionately between hemispheres such that when sea level fall reaches -180 m there is 75 m in the ice sheet of the Southern Hemisphere and 105 m in the Northern Hemisphere.

The climate forcing due to sea level changes in the two hemispheres, SL_S and SL_N, is

$$F_{Albedo}\ (W/m^2) = -2\ (SL_S/75\ m)^{4/5} - 3.5\ (SL_N/105\ m)^{4/5}, \qquad (S1)$$

where the climate forcings due to fully glaciated Antarctica (-2 W/m^2) and Northern Hemisphere glaciation during the last glacial maximum (-3.5 W/m^2) were derived from global climate model simulations (13).

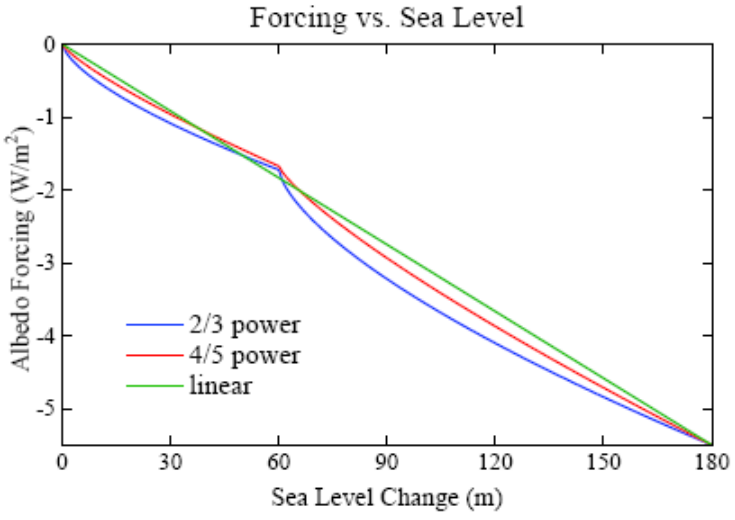

Fig. S4. Surface albedo climate forcing as a function of sea level for three approximations of the ice sheet area as a function of sea level change, from an ice free planet to the last glacial maximum. For sea level between 0 and 60 m only Antarctica contributes to the albedo change. At the last glacial maximum Antarctica contains 75 m of sea level and the Northern Hemisphere contains 105 m.

Figure S4 compares results from the present approach with results from the same approach using exponent 2/3 rather than 4/5, and with a simple linear relationship between the total forcing and sea level change. Use of exponent 4/5 brings the results close to the linear case, suggesting that the simple linear relationship is a reasonably good approximation. The similarity of Fig. 1c in our present paper and Fig. 2c in (7) indicates that change of exponent from 2/3 to 4/5 did not have a large effect.

Global nature of major climate changes. Climate changes often begin in a specific hemisphere, but the large climate changes are invariably global, in part because of the global GHG feedback. Even without the GHG feedback, forcings that are located predominately in one hemisphere, such as ice sheet changes or human-made aerosols, still evoke a global response (11), albeit with the response being larger in the hemisphere of the forcing. Both the atmosphere and ocean transmit climate response between hemispheres. The deep ocean can carry a temperature change between hemispheres with little loss, but because of the ocean's thermal inertia there can be a hemispheric lag of up to a millennium (see Ocean Response Time, below).

Figure S5 compares temperature change in Antarctica (S6), the tropical sea surface (S7), and the global deep ocean (24). Temperature records are multiplied by specific factors intended to convert the temperature record to an estimate of global temperature change. Based on paleoclimate records, polar temperature change is typically twice the global average temperature change, and tropical temperature change is about two-thirds of the global mean change. This polar amplification of the temperature change is an expected consequence of feedbacks (13), especially the snow-ice albedo feedback. The empirical result that deep ocean temperature changes are only about two-thirds as large as global temperature change is obtained from data for the Pleistocene epoch, when deep ocean temperature change is limited by its approach to the freezing point.

Holocene climate forcings. The GHG zero-point for the paleo portion of Fig. 2 is the mean for 10-8 ky BP, a time that should precede any significant anthropogenic effect on GHG amount. It has been suggested that the increase of CO_2 that began 8000 years ago is due to deforestation and the increase of CH_4 that began 6000 years ago is caused by rice agriculture (59). Regardless of whether late Holocene CO_2 and CH_4 changes are human-made, the GHG forcing is anomalous in that period relative to global temperature change estimated from ocean and ice cores. As

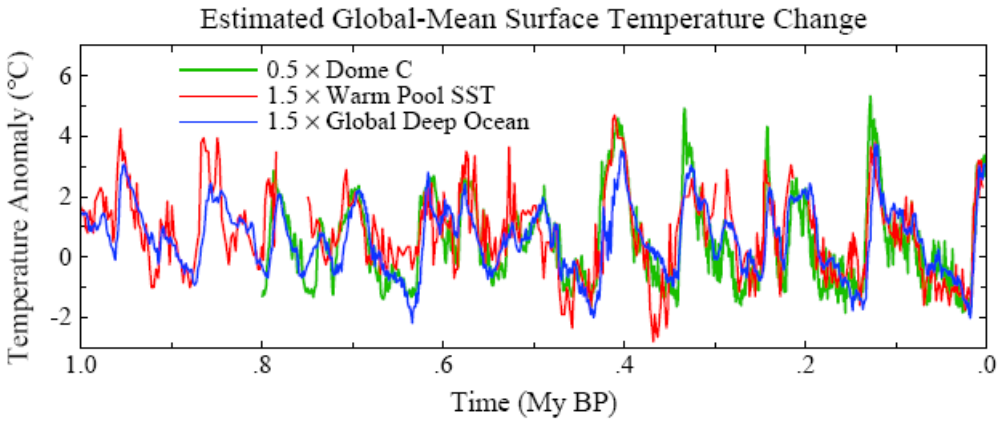

Fig. S5. Estimated global temperature change based on measurements at a single point or, in the case of the deep ocean, a near-global stack of ocean drilling sites: Antarctica Dome C (S6), Warm Pool (S7), deep ocean (24).

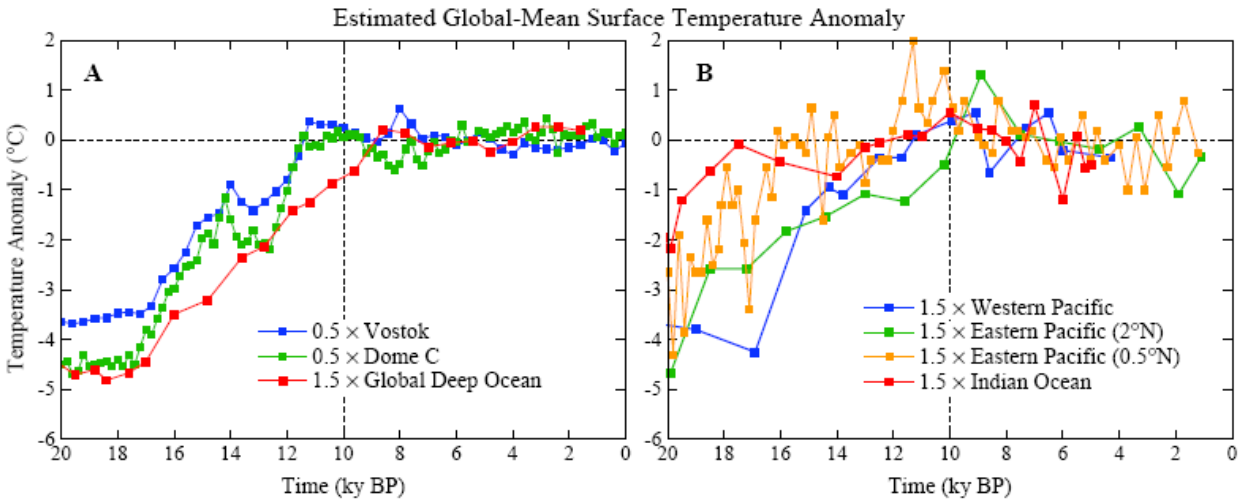

Fig. S6. Estimates of global temperature change inferred from Antarctic ice cores (27, S6) and ocean sediment cores (S7-S11), as in Fig. 5 but for a period that allows the Holocene temperature change to be apparent.

discussed elsewhere (7), the late Holocene is the only time in the ice core record in which the temperature change deviates from that expected due to GHG and surface albedo forcings.

The GHG forcing increase in the second half of the Holocene is ~3/4 W/m^2. Such a large forcing, by itself, would create a planetary energy imbalance that could not be sustained for millennia without causing a large global temperature increase, the expected global warming being about 1°C. Actual global temperature change in this period was small, perhaps a slight cooling. Figure S6 shows estimates of global temperature change obtained by dividing polar temperature change by two or multiplying tropical and deep ocean temperatures by 1.5. Clearly the Earth has not been warming rapidly in the latter half of the Holocene. Thus a substantial (negative) forcing must have been operating along with the positive GHG forcing.

Deforestation causes a negative climate forcing (11), but an order of magnitude too small to balance GHG positive forcing. A much larger negative forcing is expected from human-made aerosols. Aerosol forcing is non-linear, especially the indirect effect on clouds, with aerosols added to a pristine atmosphere being more effective than those added to the current highly polluted atmosphere. Given estimates of a negative forcing of 1-2 W/m^2 for today's anthropogenic aerosols (2, 5, 11), a negative aerosol forcing at least of the order of 0.5 W/m^2 in 1850 is expected. We conclude that aerosols were the predominant negative forcing that opposed the rapid increase of positive GHG forcing in the late Holocene.

The suggestion (59) that GHG increase in the latter half of the Holocene was due to deforestation, fires, and agricultural activities has been criticized on the grounds that the required human-made carbon transfers are unrealistically large (S12). Our present analysis relates to this discussion in several ways.

First, we have shown (Fig. 2) that the paleoclimate global temperature changes are accounted for by the atmospheric and surface albedo 'forcings" (which are slow climate feedbacks). Insolation changes due to Earth orbital changes have negligible direct forcing; they operate by instigating surface and atmospheric changes, which are the mechanisms causing global temperature change. The relevance of this observation is that the presumed human-made carbon transfers (59, S12) were based on an assumption that changes of atmospheric CO_2 and CH_4 are

proportional to insolation changes, resulting in a presumed requirement of 40 ppm CO_2 and 250 ppb CH_4 of human-made gases. However, CO_2 and CH_4 are accurately determined by global temperature, as shown individually for CO_2 and CH_4 in Figure 6 of (6). Thus the required carbon sources are only the observed increases (~20 ppm CO_2 and 100 ppb CH_4). In order for humans to be the dominate cause of the Holocene CO_2 increase they need only account for at least 10 ppm of CO_2, not 40 ppm. Thus carbon isotope analyses (S12) disproving a 40 ppm deforestation source do not contradict the hypothesis that the human impact on atmospheric composition began 6000-8000 years ago.

Second, our GHG-temperature comparison for the period of ice core data (Fig. 2) also show that the anomalous (contrary to flat or slightly decreasing temperature) leap in GHG forcing in the past 6000-8000 years is highly unusual, indeed, unique among the interglacial periods. Thus our analysis supports Ruddiman's (59) hypothesis that significant human effects began several thousand years ago.

Third, our results do not support the contention (59) that human-made forcings averted an ice age. Until the past few decades the net human-made forcing was small and of uncertain sign, as positive GHG and negative aerosol forcings were comparable in magnitude. Today the net human-made forcing is positive and growing rapidly, because CO_2 is continuing to accumulate while global aerosol amounts are stabilizing. Thus the question of when the Earth would have entered the next ice age, if there were no humans on the planet, is rhetorical and of limited interest. Human-made CO_2 will remain in the air for many millennia, eliminating the possibility of another ice age on time scales of interest to humans. Even without CO_2 an ice age could be averted with a small amount of trace gases such as chlorofluorocarbons, so there is no reason that another ice age need occur as long as long as humans and a technological society remain on the planet. The question instead is whether GHGs can be kept to a level such that climate remains close to conditions of the Holocene, or whether changes are initiated that carry the climate to a very different planetary state, one that is foreign to human experience.

Ocean response time. Figure S7 shows the climate response function, defined as the fraction of equilibrium global warming that is obtained as a function of time. This response function was obtained (7) from a 3000-year simulation after instant doubling of atmospheric CO_2, using GISS modelE (S3, 11) coupled to the Russell ocean model (S13). Note that although 40% of the equilibrium solution is obtained within several years, only 60% is achieved after a century, and

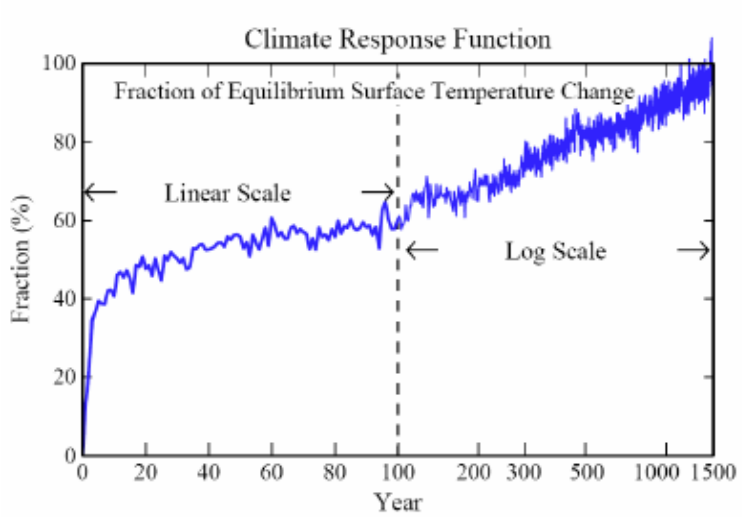

Fig. S7. Fraction of equilibrium surface temperature response versus time in the GISS climate model (7, 11, S3) with the Russell (S13) ocean. The forcing was doubled atmospheric CO_2. The ice sheets, vegetation distribution and other long-lived GHGs were fixed.

nearly full response requires a millennium. The long response time is caused by slow uptake of heat by the deep ocean, which occurs primarily in the Southern Ocean.

This delay of the surface temperature response to a forcing, caused by ocean thermal inertia, is a strong (quadratic) function of climate sensitivity and it depends on the rate of mixing of water into the deep ocean (29). The ocean model used for Fig. S7 may mix somewhat too rapidly in the waters around Antarctica, as judged by transient tracers (S13), reducing the simulated surface response on the century time scale. However, this uncertainty does not qualitatively alter the shape of the response function (Fig. S7).

When the climate model used to produce Fig. S7 is driven by observed changes of GHGs and other forcings it yields good agreement with observed global temperature and ocean heat storage (5). The model has climate sensitivity ~3°C for doubled CO_2, in good agreement with the fast-feedback sensitivity inferred from paleoclimate data.

Separation of $\delta^{18}O$ into ice volume and temperature. $\delta^{18}O$ of benthic (deep ocean dwelling) foraminifera is affected by both deep ocean temperature and continental ice volume. Between 34 My and the last ice age (20 ky) the change of $\delta^{18}O$ was ~ 3, with T_{do} change ~ 6°C (from +5 to -1°C) and ice volume change ~ 180 msl (meters of sea level). Based on the rate of change of $\delta^{18}O$ with deep ocean temperature in the prior period without land ice, ~ 1.5 of $\delta^{18}O$ is associated with the T_{do} change of ~ 6°C, and we assign the remaining $\delta^{18}O$ change to ice volume linearly at the rate 60 msl per mil $\delta^{18}O$ change (thus 180 msl for $\delta^{18}O$ between 1.75 and 4.75).

Thus we assume that ice sheets were absent when $\delta^{18}O < 1.75$ with sea level 75 msl higher than today. Sea level at smaller values of $\delta^{18}O$ is given by

$$SL\ (m) = 75 - 60 \times (\delta^{18}O - 1.75). \qquad (S2)$$

Figure S8 shows that the division of $\delta^{18}O$ equally into sea level change and deep ocean temperature captures well the magnitude of the major glacial to interglacial changes.

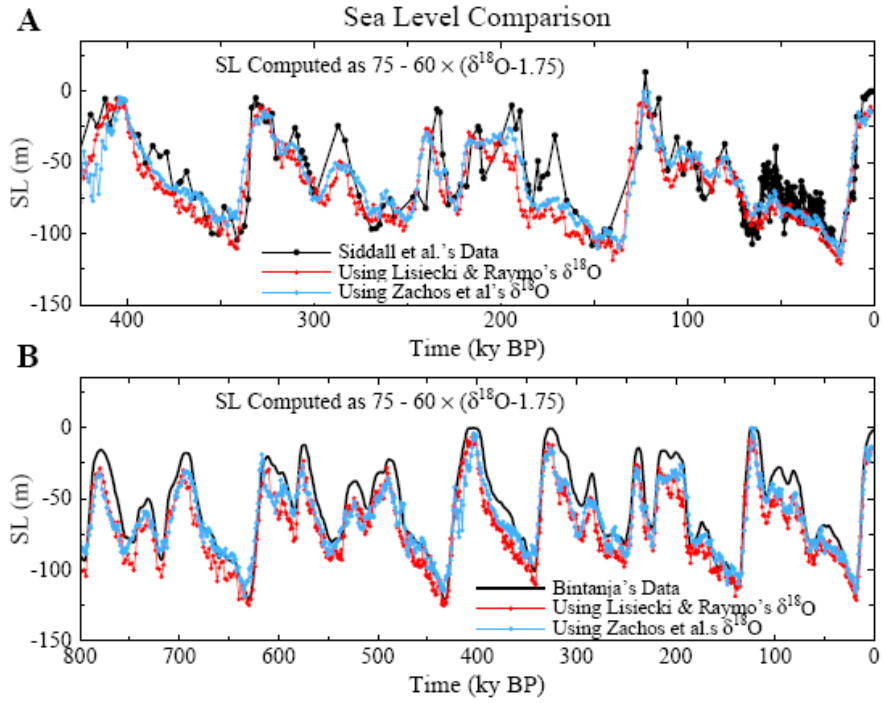

Fig. S8. (A) Comparison of Siddall *et al.* (17) sea level record with sea level computed from $\delta^{18}O$ via Eq. S2 using two alternative global benthic stacks (24, S14). (B) Comparison of Bintanja *et al.* (S15) sea level reconstruction with the same global benthic stacks as in (A).

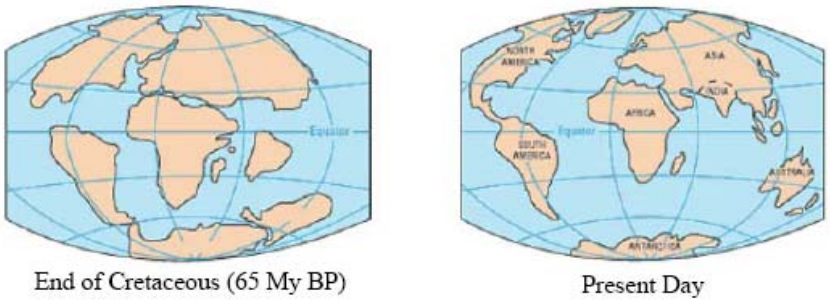

Fig. S9. Continental locations at the beginning and end of the Cenozoic era (S16).

Continental drift and atmospheric CO_2. At the beginning of the Cenozoic era 65 My ago the continents were already close to their present latitudes, so the effect of changing continental location per se did not have a large effect on the planet's energy balance (Fig. S9). However, continental drift has a major effect on the balance, or imbalance, of uptake and outgassing of CO_2 by the solid Earth. Outgassing, which occurs in regions of volcanic activity, depends upon the rate at which carbonate-rich oceanic crust is subducted beneath moving continental plates (45). Drawdown of atmospheric CO_2 occurs with weathering of rocks exposed by uplift, with the weathering products carried by rivers to the ocean and eventually deposited as carbonates on the ocean floor (46).

At the beginning of the Cenozoic the African plate was already in collision with Eurasia, pushing up the Alps. India was still south of the equator, but moving north rapidly through a region with fresh carbonate deposits. It is likely that subduction of carbonate rich crust of the Tethys Ocean, long a depocenter for sediments, caused an increase of atmospheric CO_2 and the early Cenozoic warming that peaked ~50 My ago. The period of rapid subduction terminated with the collision of India with Eurasia, whereupon uplift of the Himalayas and the Tibetan Plateau greatly increased weathering rates and drawdown of atmospheric CO_2 (49).

Since 50 My ago the major rivers of the world have emptied into the Indian and Atlantic Oceans. But there is little subduction of oceanic crust associated with the ocean basins in which these sediments are accumulating (45). Thus the present continental geography is the presumed cause of CO_2 drawdown and cooling over the past 50 My.

Proxy CO_2 data. Strengths and weaknesses of the four paleo-CO_2 reconstruction methods reported in Fig S10, discussed in detail elsewhere (S17), constrain their utility for rigorously evaluating the CO_2 predictions. In brief, the paleosol method is based on the $\delta^{13}C$ of pedogenic carbonate nodules, whose formation can be represented by a two end-member mixing model between atmospheric CO_2 and soil-derived carbon (S18). Variables that need to be constrained or assumed include an estimation of nodule depth from the surface of the original soil, the respiration rate of the ecosystem that inhabits the soil, the porosity/diffusivity of the original soil, and the isotopic composition of the vegetation contribution of respired CO_2. The uncertainties in CO_2 estimates with this proxy are substantial at high CO_2 (±500-1000 ppm when CO_2 > 1000 ppm) and somewhat less in the lower CO_2 range (±400-500 ppm when CO_2 < 1000 ppm).

The stomatal method is based on the genetically-controlled relationship (S19) between the proportion of leaf surface cells that are stomata and atmospheric CO_2 concentrations (S20). The error terms with this method are comparatively small at low CO_2 (< ±50 ppm), but the method rapidly loses sensitivity at high CO_2 (> 500-1000 ppm). Because stomatal-CO_2 relationships are often species-specific, only extant taxa with long fossil records can be used (S21). Also, because the fundamental response of stomata is to the partial pressure of CO_2 (S22), constraints on

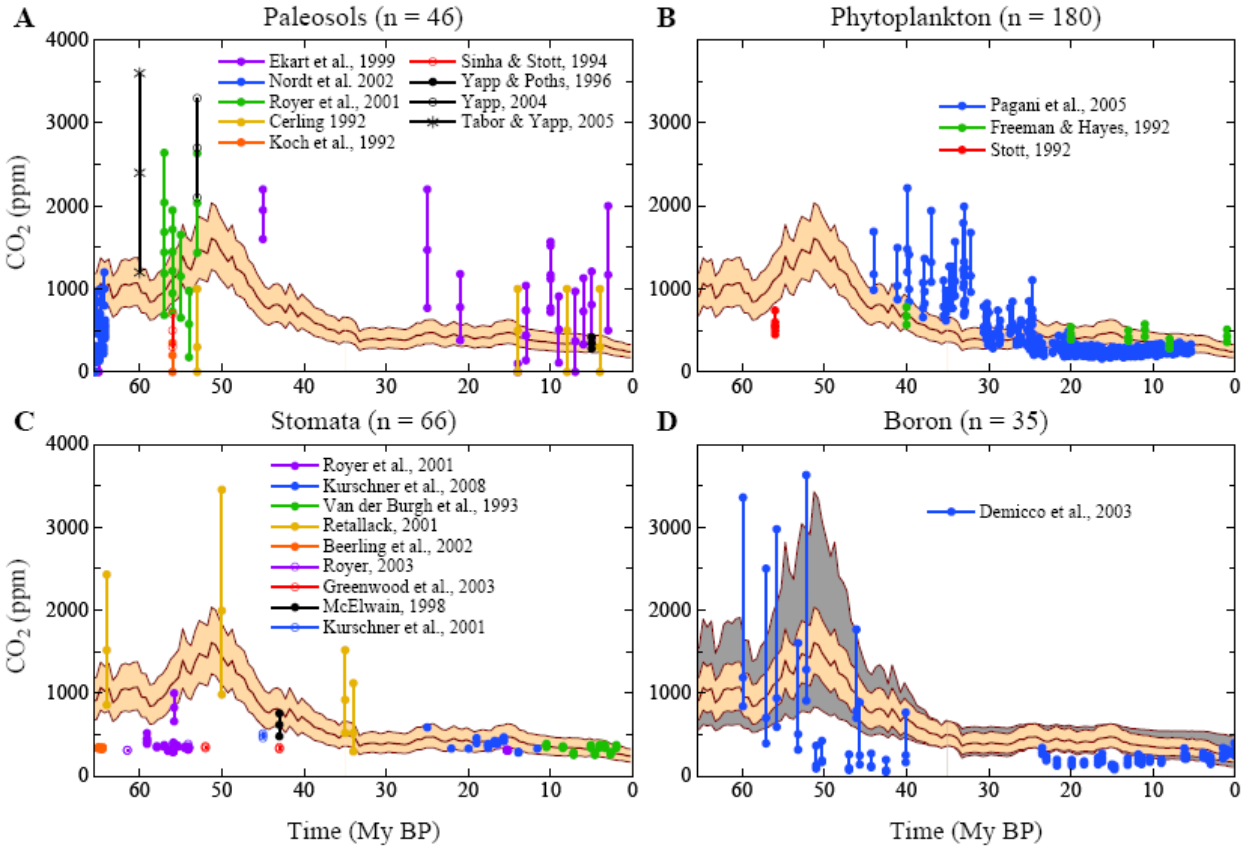

Fig. S10. Comparison of proxy CO_2 measurements with CO_2 predictions based on deep-ocean temperature, the latter inferred from benthic $\delta^{18}O$. The beige range of model results, intended only to guide the eye in comparing different proxies, is for the case $T_s = T_{do}$, the dark central line for the case CO_2 = 450 ppm at 34 My ago and the borders of the beige area being 325 and 600 ppm. Part D shows the additional range in the model prediction for a 50% uncertainty in the relationship of T_s and T_{do}. Our assumption that CO_2 provides 75% of the GHG throughout the Cenozoic adds additional uncertainty to the predicted CO_2 amount.

paleoelevation are required.

The phytoplankton method is based on the Rayleigh distillation process of fractionating stable carbon isotopes during photosynthesis (S23). In a high CO_2 environment, for example, there is a higher diffusion rate of CO_2 through phytoplankton cell membranes, leading to a larger available intercellular pool of $CO_{2[aq]}$ and more depleted $\delta^{13}C$ values in photosynthate. Cellular growth rate and cell size also impact the fractionation of carbon isotopes in phytoplankton and thus fossil studies must take these factors into account (S24). This approach to reconstructing CO_2 assumes that the diffusional transport of CO_2 into the cell dominates, and that any portion of carbon actively transported into the cell remains constant with time. Error terms are typically small at low CO_2 (< ±50 ppm) and increase substantially under higher CO_2 concentrations (S24).

The boron-isotope approach is based on the pH-dependency of the $\delta^{11}B$ of marine carbonate (S25). This current method assumes that only borate is incorporated in the carbonate lattice and that the factionation factor for isotope exchange between boric acid and borate in solution is well-constrained. Additional factors that must be taken into account include test dissolution and size, species-specific physiological effects on carbonate $\delta^{11}B$, and ocean alkalinity (S26-28). As with the stomatal and phytoplankton methods, error terms are comparatively small at low CO_2

Table S1. Climate sensitivities inferred semi-empirically from Cenozoic or Phanerozoic climate change.

Reference	Period	Doubled CO_2 Sensitivity
Royer et al. (53)	0-420 My	~ 2.8°C
Higgins and Schrag (54)	PETM	~4°C
Pagani et al. (55)	PETM	High

(< ±50 ppm) and the method loses sensitivity at higher CO_2 (> 1000 ppm). Uncertainty is unconstrained for extinct foraminiferal species.

Climate sensitivity comparisons. Other empirical or semi-empirical derivations of climate sensitivity from paleoclimate data (Table S1) are in reasonable accord with our results, when account is taken of differences in definitions of sensitivity and the periods considered.

Royer et al. (53) use a carbon cycle model, including temperature dependence of weathering rates, to find a best-fit doubled CO_2 sensitivity of 2.8°C based on comparison with Phanerozoic CO_2 proxy amounts. Best-fit in their comparison of model and proxy CO_2 data is dominated by the times of large CO_2 in the Phanerozoic, when ice sheets would be absent, not by the times of small CO_2 in the late Cenozoic. Their inferred sensitivity is consistent with our inference of ~3°C for doubled CO_2 at times of little or no ice on the planet.

Higgins and Schrag (54) infer climate sensitivity of ~4°C for doubled CO_2 from the temperature change during the Paleocene-Eocene Thermal Maximum (PETM) ~55 My ago Fig.

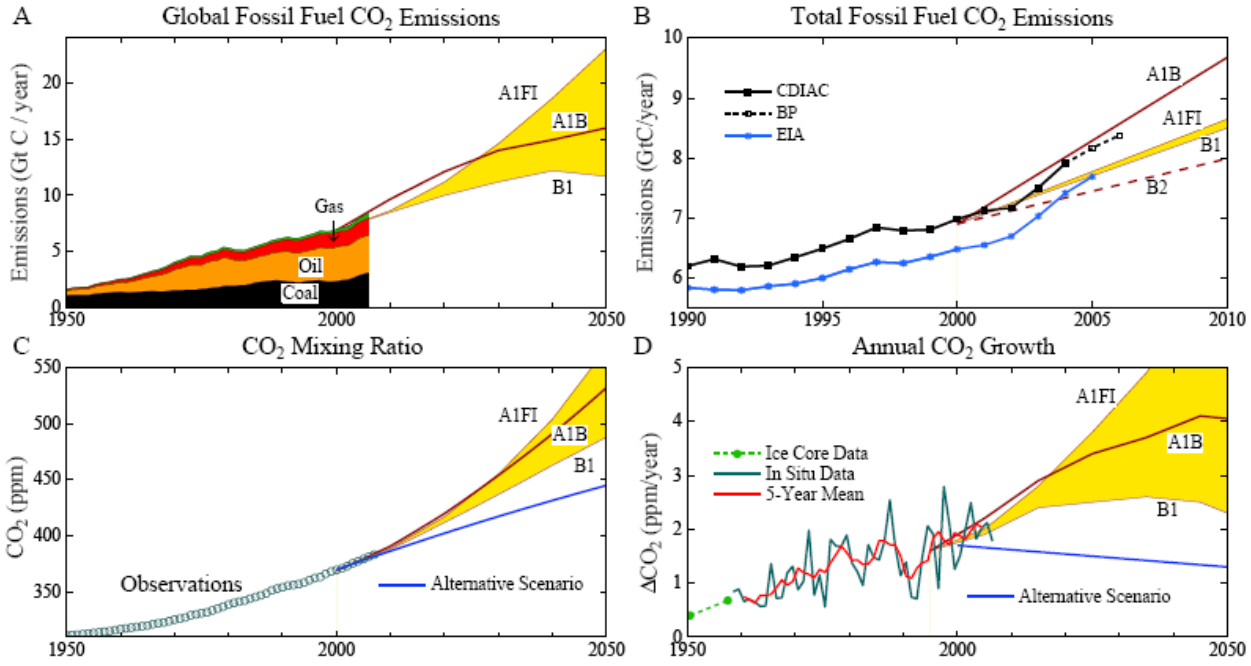

Fig. S11. (A) Fossil fuel CO_2 emissions by fuel type (S29, S30), the thin green sliver being gas flaring plus cement production, and IPCC fossil fuel emissions scenarios, (B) expansion global emissions to show recent changes more precisely, the EIA values excluding CO_2 emissions from cement manufacture, (C) observed atmospheric CO_2 amount and IPCC and "alternative" scenarios for the future, (D) annual atmospheric CO_2 growth rates. Data here is an update of data sources defined in (6). The yellow area is bounded by scenarios that are most extreme in the second half of the 21st century; other scenarios fall outside this range in the early part of the century.

3), based on the magnitude of the carbon isotope excursion at that time. Their climate sensitivity for an ice-free planet is consistent with ours within uncertainty ranges. Furthermore, recalling that we assume non-CO_2 to provide 25% of the GHG forcing, if one assumes that part of the PETM warming was a direct of effect of methane, then their inferred climate sensitivity is in even closer agreement with ours.

Pagani et al. (55) also use the magnitude of the PETM warming and the associated carbon isotopic excursion to discuss implications for climate sensitivity, providing a graphical relationship to help assess alternative assumptions about the origin and magnitude of carbon release. They conclude that the observed PETM warming of about 5°C implies a high climate sensitivity, but with large uncertainty due to imprecise knowledge of the carbon release.

Greenhouse gas growth rates. Fossil fuel CO_2 emissions have been increasing at a rate close to the highest IPCC (S31) scenario (Fig. S11B). Increase of CO_2 in the air, however, appears to be in the middle of the IPCC scenarios (Fig. S11C, D), but as yet the scenarios are too close and interannual variability too large, for assessment. CO_2 growth is well above the "alternative scenario", which was defined with the objective of keeping added GHG forcing in the 21st century at about 1.5 W/m^2 and 21st century global warming less than 1°C (18).

Non-CO_2 greenhouse gases are increasing more slowly than in IPCC scenarios, overall at approximately the rate of the "alternative scenario", based on a review of data through the end of 2007 (67). There is potential to reduce non-CO_2 forcings below the alternative scenario (67).

Fossil fuel and land-use CO_2 emissions. Figure S12 shows estimates of anthropogenic CO_2 emissions to the atmosphere. Although fossil emissions through 2006 are known with good accuracy, probably better than 10%, reserves and potential reserve growth are highly uncertain. IPCC (S31) estimates for oil and gas proven reserves are probably a lower limit for future oil and

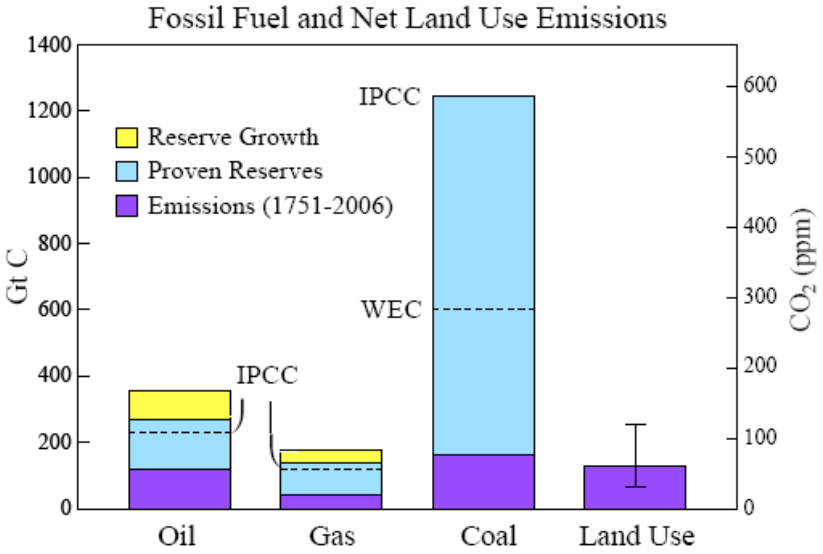

Fig. S12. Fossil fuel and land-use CO_2 emissions, and potential fossil fuel emissions. Historical fossil fuel emissions are from the Carbon Dioxide Information Analysis Center (CDIAC, S29) and British Petroleum (BP, S30). Lower limits on oil and gas reserves are from IPCC (S31) and higher limits are from the United States Energy Information Administration (EIA, 78). Lower limit for coal reserves is from the World Energy Council (WEC, S32) and upper limit from IPCC (S31). Land use estimate is from integrated emissions of Houghton/2 (Fig. S14) supplemented to include pre-1850 and post-2000 emissions; uncertainty bar is subjective.

gas emissions, but they are perhaps a feasible goal that could be achieved via a substantial growing carbon price that discourages fossil fuel exploration in extreme environments together with national and international policies that accelerate transition to carbon-free energy sources and limit fossil fuel extraction in extreme environments and on government controlled property.

Coal reserves are highly uncertain, but the reserves are surely enough to take atmospheric CO_2 amount far into the region that we assess as being "dangerous". Thus we only consider scenarios in which coal use is phased out as rapidly as possible, except for uses in which the CO_2 is captured and stored so that it cannot escape to the atmosphere. Thus the magnitude of coal reserves does not appreciably affect our simulations of future atmospheric CO_2 amount.

Integrated 1850-2008 net land-use emissions based on the full Houghton (81) historical emissions (fig. S14), extended with constant emissions for the past several years, are 79 ppm CO_2. Although this could be an overestimate by up to a factor of two (see below), substantial pre-1850 deforestation must be added in. Our subjective estimate of uncertainty in the total land-use CO_2 emission is a factor of two.

The modern carbon cycle. Atmospheric CO_2 amount is affected significantly not only by fossil fuel emissions, but also by agricultural and forestry practices. Quantification of the role of land-use in the uptake and release of CO_2 is needed to assess strategies to minimize human-made climate effects.

Figure S13 shows the CO_2 airborne fraction, AF, the annual increase of atmospheric CO_2 divided by annual fossil fuel CO_2 emissions. AF is a critical metric of the modern carbon cycle, because it is based on the two numbers characterizing the global carbon cycle that are well known. AF averages 56% over the period of accurate data, which began with the CO_2 measurements of Keeling in 1957, with no discernable trend. The fact that 44% of fossil fuel emissions seemingly "disappears" immediately provides a hint of optimism with regard to the possibility of stabilizing, or reducing, atmospheric CO_2 amount.

That optimism needs to be tempered, as we will see, by realization of the magnitude of the actions required to halt and reverse CO_2 growth. However, it is equally important to realize that assertions that fossil fuel emissions must be reduced close to 100% on an implausibly fast schedule are not necessarily valid.

A second definition of the airborne fraction, AF2, is also useful. AF2 includes the net anthropogenic land-use emission of CO_2 in the denominator. This AF2 definition of airborne fraction has become common in recent carbon cycle literature. However, AF2 is not an observed or accurately known quantity; it involves estimates of net land-use CO_2 emissions, which vary among investigators by a factor of two or more (2).

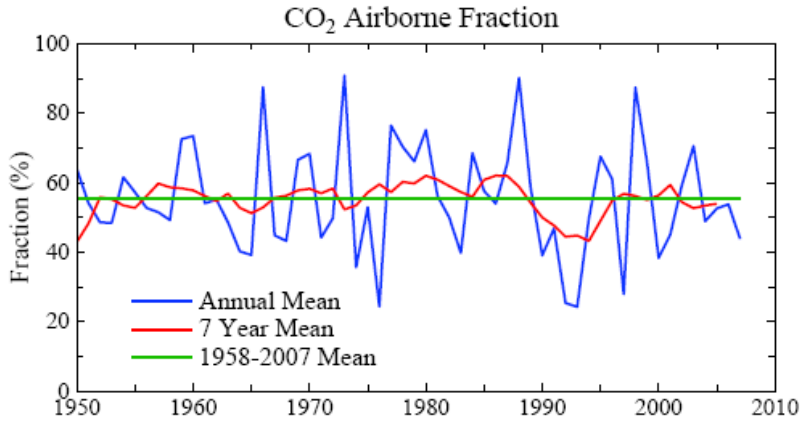

Fig. S13. CO_2 airborne fraction, AF, the ratio of annual observed atmospheric CO_2 increase to annual fossil fuel CO_2 emissions.

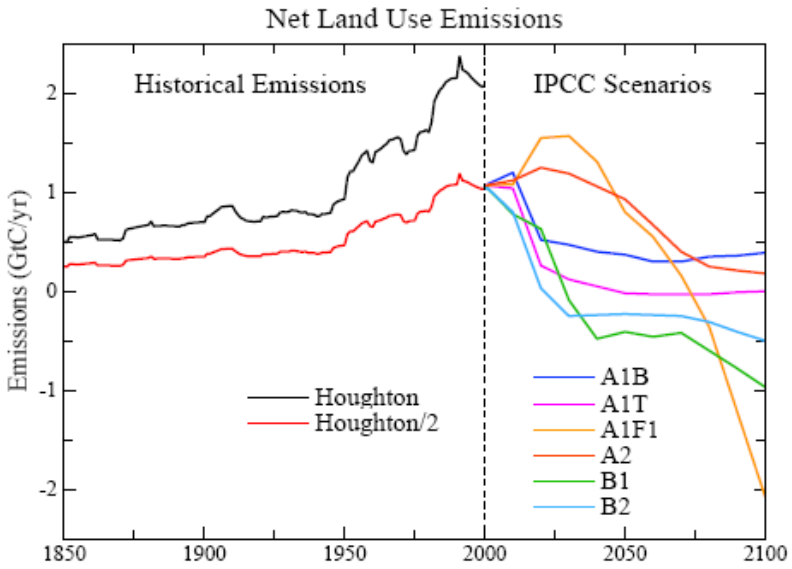

Fig. S14. Left side: estimate by Houghton et al. (81) of historical net land-use CO_2 emissions, and a 50 percent reduction of that estimate. Right side: IPCC (2) scenarios for land-use CO_2 emissions.

Figure S14 shows an estimate of net land-use CO_2 emissions commonly used in carbon cycle studies, labeled "Houghton" (81), as well as "Houghton/2", a 50% reduction of these land-use emissions. An over-estimate of land-use emissions is one possible solution of the long-standing "missing sink" problem that emerges when the full "Houghton" land-use emissions are employed in carbon cycle models (2, S31, 77).

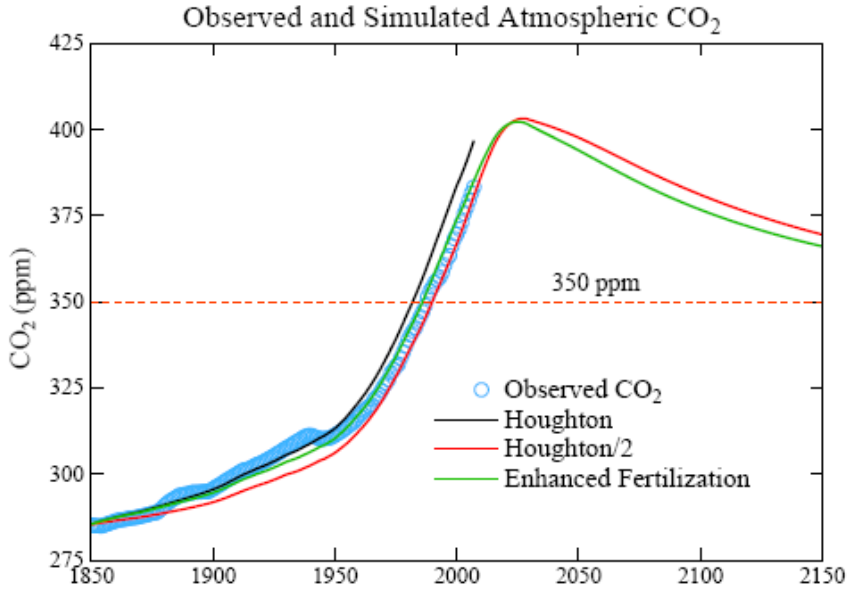

Fig. S15. Computed and observed time evolution of atmospheric CO_2. "Enhanced Fertilization" uses the full "Houghton" land use emissions for 1850–2000. "Houghton/2" and "Enhanced Fertilization" simulations are extended to 2100 assuming coal phase-out by 2030 and the IPCC (2) A1T land-use scenario. Observations are from Law Dome ice core data and flask and in-situ measurements (6, S33, http://www.esrl.noaa.gov/gmd/ccgg/trends/).

Principal competing solutions of the "missing sink" paradox are (1) land-use CO_2 emissions are over-estimated by about a factor of two, or (2) the biosphere is being "fertilized" by anthropogenic emissions, via some combination of increasing atmospheric CO_2, nitrogen deposition, and global warming, to a greater degree than included in typical carbon cycle models. Reality may include contributions from both candidate explanations. There is also a possibility that imprecision in the ocean uptake of CO_2, or existence of other sinks such as clay formation, could contribute increased CO_2 uptake, but these uncertainties are believed to be small.

Figure S15 shows resulting atmospheric CO_2, and Figure S16 shows AF and AF2, for two extreme assumptions: "Houghton/2" and " Enhanced Fertilization", as computed with a dynamic-sink pulse response function (PRF) representation of the Bern carbon cycle model (76, 77). Fertilization is implemented via a parameterization (76) that can be adjusted to achieve an improved match between observed and simulated CO_2 amount. In the "Houghton/2" simulation the original value (76) of the fertilization parameter is employed while in the "Enhanced Fertilization" simulation the full Houghton emissions are used with a larger fertilization parameter. Both "Houghton/2" and "Enhanced Fertilization" yield good agreement with the observed CO_2 history, but Houghton/2 does a better job of matching the time dependence of observed AF.

It would be possible to match observed CO_2 to an arbitrary precision if we allowed the adjustment to "Houghton" land-use to vary with time, but there is little point or need for that. Fig. S15 shows that projections of future CO_2 do not differ much even for the extremes of Houghton/2 and Enhanced Fertilization. Thus in Figure 6 we show results for only the case Houghton/2, which is in better agreement with the airborne fraction and also is continuous with IPCC scenarios for land use.

Implications of Figure 6: CO_2 Emissions and Atmospheric Concentration with Coal Phase-out by 2030. Figure 6 provides an indication of the magnitude of actions that are needed to return atmospheric CO_2 to a level of 350 ppm or lower. Figure 6 allows for the fact that there is disagreement about the magnitude of fossil fuel reserves, and that the magnitude of useable reserves depends upon policies.

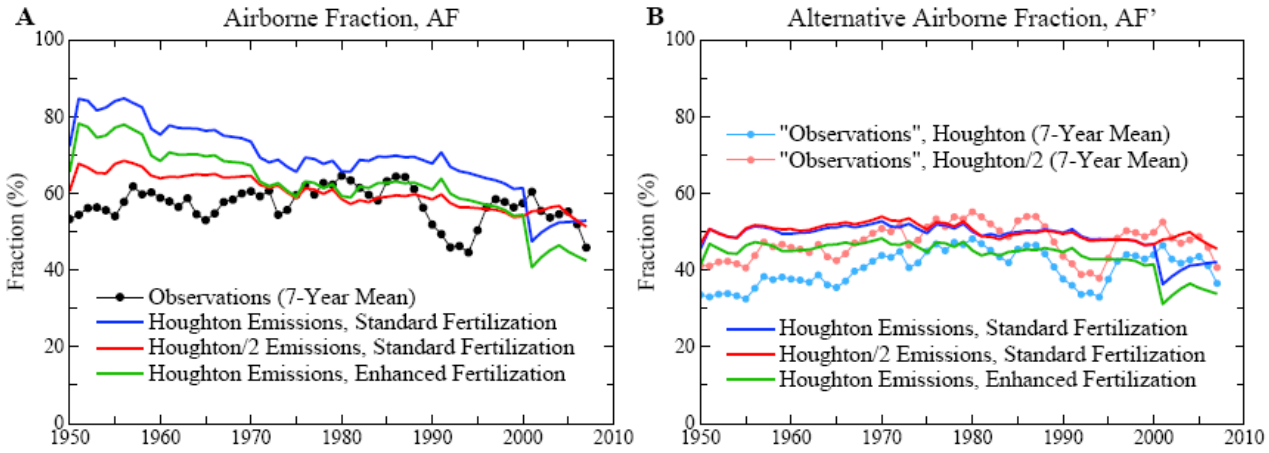

Fig. S16. (A) Observed and simulated airborne fraction (AF), the ratio of annual CO_2 increase in the air over annual fossil fuel CO_2 emissions, (B) AF2 includes the sum of land use and fossil fuel emissions in the denominator in defining airborne fraction; thus AF2 is not accurately known because of the large uncertainty in land use emissions.

A basic assumption underlying Figure 6 is that, within the next several years, there will be a moratorium on construction of coal-fired power plants that do not capture and store CO_2, and that CO_2 emissions from existing power plants will be phased out by 2030. This coal emissions phase out is the sine qua non for stabilizing and reducing atmospheric CO_2. If the sine qua non of coal emissions phase-out is achieved, atmospheric CO_2 can be kept to a peak amount ~400-425 ppm, depending upon the magnitude of oil and gas reserves.

Figure 6 illustrates two widely different assumptions about the magnitude of oil and gas reserves (illustrated in fig. S12). The smaller oil and gas reserves, those labeled "IPCC", are realistic if "peak oil" advocates are more-or-less right, i.e., if the world has already exploited about half of readily accessible oil and gas deposits, so that production of oil and gas will begin to decline within the next several years.

There are also "resource optimists" who dispute the "peakists', arguing that there is much more oil (and gas) to be found. It is possible that both the "peakists" and "resource optimists" are right, it being a matter of how hard we work to extract maximum fossil fuel resources. From the standpoint of controlling human-made climate change, it does not matter much which of these parties is closer to the truth.

Figure 6 shows that, if peak CO_2 is to be kept close to 400 ppm, the oil and gas reserves actually exploited need to be close to the "IPCC" reserve values. In other words, if we phase out coal emissions we can use remaining oil and gas amounts equal to those which have already been used, and still keep peak CO_2 at about 400 ppm. Such a limit is probably necessary if we are to retain the possibility of a drawdown of CO_2 beneath the 350 ppm level by methods that are more-or-less "natural". If, on the other hand, reserve growth of the magnitude that EIA estimates (Figs. 6 and S12) occurs, and if these reserves are burned with the CO_2 emitted to the atmosphere, then the forest and soil sequestration that we discuss would be inadequate to achieve drawdown below the 350 ppm level in less than several centuries.

Even if the greater resources estimated by EIA are potentially available, it does not mean that the world necessarily must follow the course implied by EIA estimates for reserve growth. If a sufficient price is applied to carbon emissions it will discourage extraction of fossil fuels in the most extreme environments. Other actions that would help keep effective reserves close to the IPCC estimates would include prohibition of drilling in environmentally sensitive areas, including the Arctic and Antarctic.

National policies, in most countries, have generally pushed to expand fossil fuel reserves as much as possible. This might partially account for the fact that energy information agencies, such as the EIA in the United States, which are government agencies, tend to forecast strong growth of fossil fuel reserves. On the other hand, state, local, and citizen organizations can influence imposition of limits on fossil fuel extraction, so there is no guarantee that fossil resources will be fully exploited. Once the successors to fossil energy begin to take hold, there may be a shifting away from fossil fuels that leaves some of the resources in the ground. Thus a scenario with oil and gas emissions similar to that for IPCC reserves may be plausible.

Assumptions yielding the Forestry & Soil wedge in Figure 6B are as follows. It is assumed that current net deforestation will decline linearly to zero between 2010 and 2015. It is assumed that uptake of carbon via reforestation will increase linearly until 2030, by which time reforestation will achieve a maximum potential sequestration rate of 1.6 GtC per year (S34). Waste-derived biochar application will be phased in linearly over the period 2010-2020, by which time it will reach a maximum uptake rate of 0.16 GtC/yr (83). Thus after 2030 there will be an annual uptake of 1.6 + 0.16 = 1.76 GtC per year, based on the two processes described.

Thus Figure 6 shows that the combination of (1) moratorium and phase-out of coal emissions by 2030, (2) policies that effectively keep fossil fuel reserves from significantly exceeding the IPCC reserve estimates, and (3) major programs to achieve carbon sequestration in forests and soil, can together return atmospheric CO_2 below the 350 ppm level before the end of the century.

The final wedge in Figure 6 is designed to provide an indication of the degree of actions that would be required to bring atmospheric CO_2 back to the level of 350 ppm by a time close to the middle of this century, rather than the end of the century. This case also provides an indication of how difficult it would be to compensate for excessive coal emissions, if the world should fail to achieve a moratorium and phase-out of coal as assumed as our "sine qua non".

Assumptions yielding the Oil-Gas-Biofuels wedge in Figure 6B are as follows: energy efficiency, conservation, carbon pricing, renewable energies, nuclear power and other carbon-free energy sources, and government standards and regulations will lead to decline of oil and gas emissions at 4% per year beginning when 50% of the estimated resource (oil or gas) has been exploited, rather than the 2% per year baseline decline rate (77). Also capture of CO_2 at gas-fired power plants will be phased in over the period 2010-2020, and beyond 2020 gas-fired power plants (with CO_2 capture) will use 50% of remaining gas supplies. Also a linear phase-in of liquid biofuels is assumed between 2015 and 2025 leading to a maximum global bioenergy from "low-input/high-diversity" biofuels of ~23 EJ/yr, inferred from Tilman et al. (85), that is used as a substitute for oil; this is equivalent to ~0.5 GtC/yr, based on energy conversion of 50 EJ/GtC for oil. Finally, from 2025 onward, twice this number (i.e., 1 GtC/yr) is subtracted from annual oil emissions, assuming root/soil carbon sequestration via this biofuel-for-oil substitution is at least as substantial as in Tilman et al. (85). An additional option that could contribute to this wedge is using biofuels in powerplants with CO_2 capture and sequestration (84).

EPICA 800 ky data. Antarctic Dome C ice core data acquired by EPICA (European Project for Ice Coring in Antarctica) provide a record of atmospheric composition and temperature spanning 800 ky (S6), almost double the time covered by the Vostok data (16) of Figs. 1 and 2 This extended record allows us to examine the relationship of climate forcing mechanisms and temperature change over a period that includes a substantial change in the nature of glacial-interglacial climate swings. During the first half of the EPICA record, the period 800-400 ky BP, the climate swings were smaller, sea level did not rise as high as the present level, and the GHGs did not increase to amounts as high as those of recent interglacial periods.

Figure S17 shows that the temperature change calculated exactly as described for the Vostok data of Fig. 1, i.e., multiplying the fast-feedback climate sensitivity ¾°C per W/m^2 by the sum of the GHG and surface albedo forcings (Fig. S17B), yields a remarkably close fit in the first half of the Dome C record to one-half of the temperature inferred from the isotopic composition of the ice. In the more recent half of the record slightly larger than ¾°C per W/m^2 would yield a noticeably better fit to the observed Dome C temperature divided by two (Figure S18). However, there is no good reason to change our approximate estimate of ¾°C per W/m^2, because the assumed polar amplification by a factor of two is only approximate.

The sharper spikes in recent observed interglacial temperature, relative to the calculated temperature, must be in part an artifact of differing temporal resolutions. Temperature is inferred from the isotopic composition of the ice, being a function of the temperature at which the snowflakes formed, and thus inherently has a very high temporal resolution. GHG amounts, in contrast, are smoothed over a few ky by mixing of air in the snow that occurs up until the snow is deep enough for the snow to be compressed into ice. In the central Antarctic, where both Vostok and Dome C are located, bubble closure requires a few thousand years (16).

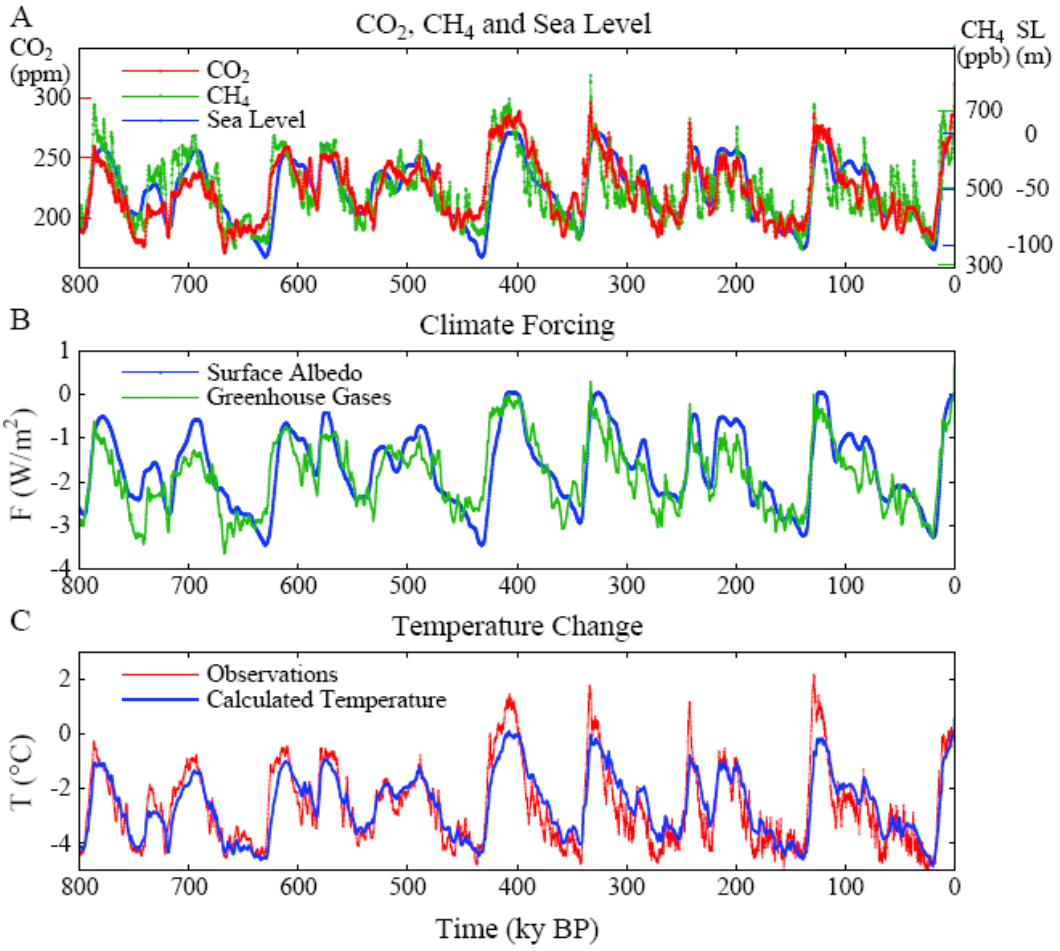

Fig. S17. (A) CO_2 (S34), CH_4 (S35) and sea level (S15) for past 800 ky. (B) Climate forcings due to changes of GHGs and ice sheet area, the latter inferred from the sea level history of Bintanja et al. (S11). (C) Calculated global temperature change based on the above forcings and climate sensitivity ¾°C per W/m^2. Observations are Antarctic temperature change from the Dome C ice core (S6) divided by two.

Sea level records used to compute the surface albedo forcing in Fig. S17B, generally, are smoothed even more than the GHG forcing. This is in part because the sea level change is inferred from $\delta^{18}O$ in ocean sediment cores. The sediments are stirred by bioturbation, resulting in a smoothing of at least several thousand years. In addition, the sea level record used for the albedo forcings in Figs. S17 and S18 (S15) was based in part on an ice sheet model, which was used to separate the ice volume and ocean temperature components of $\delta^{18}O$. The ice sheet model employed did not allow the possibility of rapid ice sheet collapse. Some sea level reconstructions based on evidence of shoreline changes suggest the existence of rapid sea level changes within interglacial periods (30), with the possibility of brief sea level high-stands as much as 9 m above present sea level (31).

Comparison of Antarctic data sets. Figure S19 compares Antarctic data sets used in this supplementary section and in our parent paper. This comparison is also relevant to interpretations of the ice core data in prior papers using the original Vostok data.

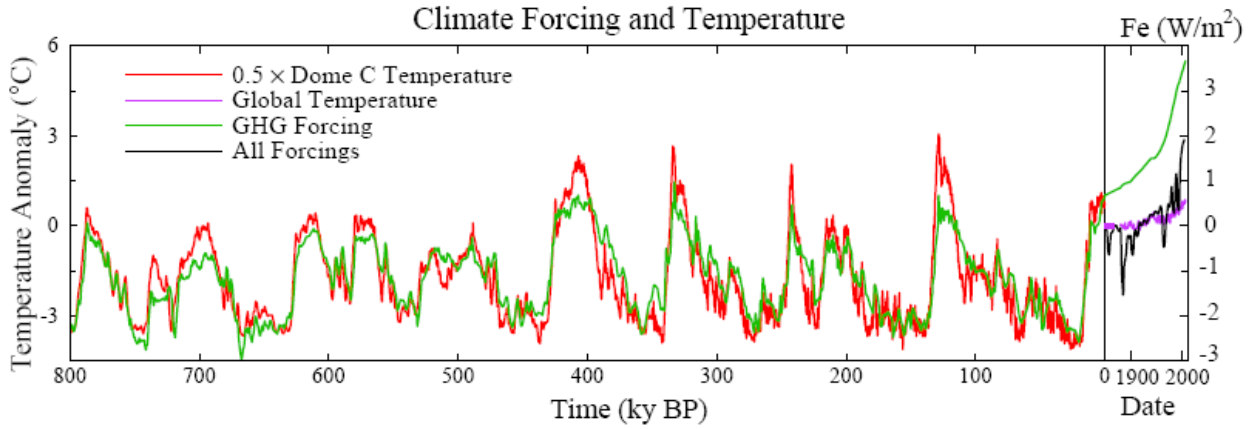

Fig. S18. Global temperature (left scale) and GHG forcing (right scale) due to CO_2, CH_4 and N_2O from Vostok ice core (16, 27). Ratio of temperature and forcing scales is 1.5°C per W/m^2. Time scale is expanded in the extension to recent years. Modern forcings include human-made aerosols, volcanic aerosols and solar irradiance (5). GHG forcing zero point is the mean for 10-8 ky before present. Net climate forcing and modern temperature zero points are at 1850. The implicit presumption that the positive GHG forcing at 1850 is largely offset by negative human-made forcings (7) is supported by the lack of rapid climate change at that time.

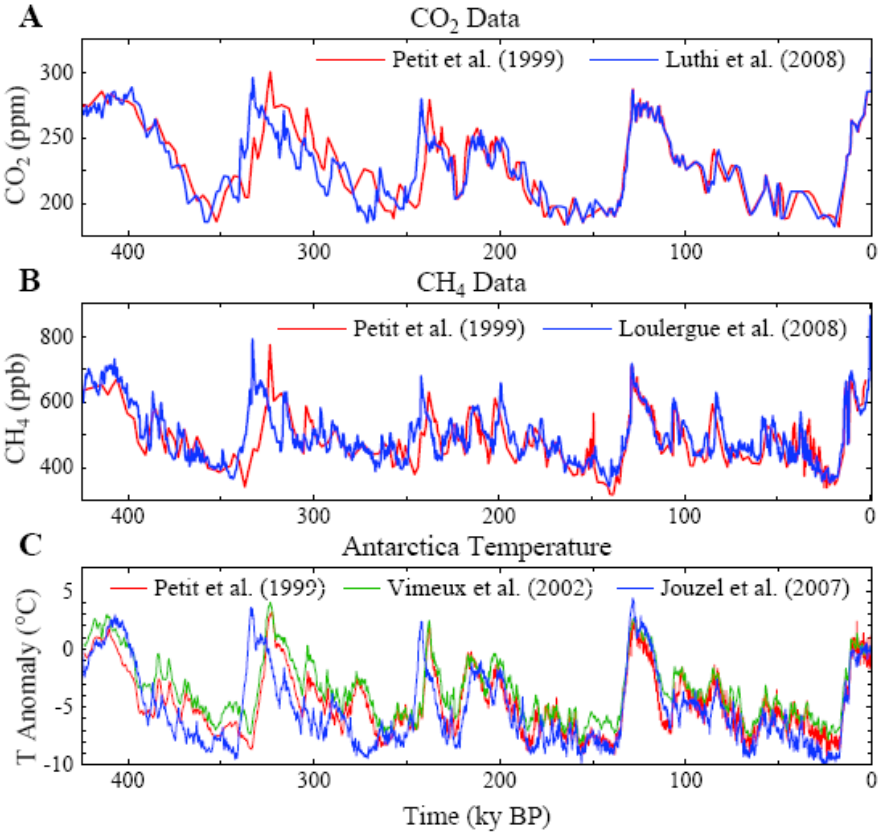

Fig. S19. Comparison of Antarctic CO_2, CH_4, and temperature records in several analyses of Antarctic ice core data.

The temperature records of Petit et al. (16) and Vimeux et al. (27) are from the same Vostok ice core, but Vimeux et al. (25) have adjusted the temperatures with a procedure designed to correct for climate variations in the water vapor source regions. The isotopic composition of the ice is affected by the climate conditions in the water vapor source region as well as by the temperature in the air above Vostok where the snowflakes formed; thus the adjustment is intended to yield a record that more accurately reflects the air temperature at Vostok. The green temperature curve in Fig. S19C, which includes the adjustment, reduces the amplitude of glacial-interglacial temperature swings from those in the original (red curve) Petit et al. (16) data. Thus it seems likely that there will be some reduction of the amplitude and spikiness of the Dome C temperature record when a similar adjustment is made to the Dome C data set.

The temporal shift of the Dome C temperature data (S6), relative to the Vostok records, is a result of the improved EDC3 (S37, S38) time scale. With this new time scale, which has a 1σ uncertainty of ~3 ky for times earlier than ~130 ky BP, the rapid temperature increases of Termination IV (~335 ky BP) and Termination III (~245 ky BP) are in close agreement with the contention (7) that rapid ice sheet disintegration and global temperature rise should be nearly simultaneous with late spring (April-May-June) insolation maxima at 60N latitude, as was already the case for Terminations II and I, whose timings are not significantly affected by the improved time scale.

The CO_2 data (Fig. S19A) used for Fig.S17 and Fig. S18 are a combined stack of Vostok (16) and Dome C (S39, S36) data on the EDC3 time scale, as presented by Luthi et al. (S35). The addition of Dome C data does not noticeably affect the amplitude of CO_2 glacial-interglacial changes. The CH_4 data (Fig. S19B) used for Figs. S17 and S18 are from the Vostok ice core (S40), but on the EDC3 time scale (S35, S36).

Supplementary References

S1. C. Hewitt, J. Mitchell, *Clim. Dyn.* **13**, 834 (1997).
S2. P. Chylek, U. Lohmann, *Geophys. Res. Lett.* **15**, L04804, doi:10.1029/2007GL032759 (2008).
S3. G.A. Schmidt *et al., J. Clim.* **19**, 153 (2006).
S4. P.F. Hoffman, D.P. Schrag, *Terra Nova* **14**, 129 (2002).
S5. M.A. Chandler, L.E. Sohl, *J. Geophys. Res.* **105**, 20737 (2000).
S6. J. Jouzel *et al., Science* **317**, 793 (2007).
S7. M. Medina-Elizade, D.W. Lea, *Science* **310**, 1009 (2005).
S8. J. Hansen *et al., Proc. Natl. Acad. Sci.* **103**, 14288 (2006).
S9. D.W. Lea, D.K. Pak, H.J. Spero, *Science*, **289**, 1719 (2000).
S10. D. W. Lea et al., *Q. Sci. Rev.*, **25**, 1152 (2006).
S11. R. Saraswat, *et al., Geophys. Res. Lett.*, **32**, L24605 (2005).
S12. W.S. Broecker, T.F. Stocker, *EOS Trans. AGU* **87**, 27 (2006).
S13. G.L. Russell, *et al., Dyn. Atmos. Oceans* **9**, 253 (1995).
S14. L.E. Lisiecki, M.E. Raymo, *Paleocean.* **20**, PA1003 (2005).
S15. R. Bintanja *et al., Nature* **437**, 125 (2005).
S16. E.A. Keller, N. Pinter, in *This Dynamic Earth: The Story of Plate Tectonics*, eds. J. Kious, R.I. Tilling, Prentice-Hall, New York, (1996).
S17. D. L. Royer, R. A. Berner, D. J. Beerling, Earth-Science Reviews 54, 349 (2001).
S18. T. E. Cerling, *Am. J. Sci.* **291**, 377 (1991).
S19. J. E. Gray *et al., Nature* **408**, 713 (2000).
S20. F. I. Woodward, *Nature* **327**, 617 (1987).
S21. D. L. Royer, *Rev. Palaeobot. Palynol.* **114**, 1 (2001).
S22. F. I. Woodward, F. A. Bazzaz, *J. Exper. Bot.* **39**, 1771 (1988).

S23. B. N. Popp, *et al., Amer. J. Sci.* **289**, 436 (1989).
S24. M. Pagani, Philosophical Transactions of the Royal Society London A 360, 609 (2002).
S25. A. J. Spivack, *et al., Nature* **363**, 149 (1993).
S26. D. Blamart *et al., Geochem., Geophys., Geosys.* **8**, Q12001, doi:10.1029/2007GC001686 (2007).
S27. D. Lemarchand, *et al., Nature* **408**, 951 (2000).
S28. M. Pagani, *et al., Geochimica et Cosmochimica Acta* **69**, 953 (2005).
S29. G. Marland, *et al., Trends*, Carbon Dioxide Information Analysis Center, Oak Ridge Nat. Lab., U.S. DOE, Oak Ridge, TN (2006).
S30. British Petroleum, *Stat. Rev. World Energy*, www.bp.com/pdf/statistical_review_of _world energy_full_report2006.pdf (2006).
S31. Intergovernmental Panel on Climate Change (IPCC), *Climate Change 2001: Mitigation*, B. Metz et al., Eds. (Cambridge Univ. Press, New York, 2001).
S32. World Energy Council (2007), *Survey of Energy Resources*, http://www.worldenergy .org/publications/survey_of_energy_resources_2007/default.asp (2007).
S33. C.D. Keeling, T.P. Whorf, Trends: *A Compendium on Global Change*, Carbon Dioxide Information Analysis Center, Oak Ridge Nat. Lab., U.S. DOE, Oak Ridge, TN (2005).
S34. Intergovernmental Panel on Climate Change (IPCC), *Land Use, Land-Use Change, and Forestry*, R.T. Watson et al., Eds. (Cambridge Univ. Press, Cambridge, UK, 2000).
S35. D. Luthi *et al., Nature* (in press).
S36. L. Loulergue, *et al., Nature* (cond. accepted, 2008).
S37. F. Parrenin, *et al., Clim. Past* **3**, 243 (2007).
S38. G. Dreyfus *et al., Clim. Past* **3**, 341 (2007).
S39. U. Siegenthaler, *et al., Science* **310**, 1313 (2005).
S40. R. Spahni *et al., Science* **310**, 1317 (2005).